AUTOMATIC BACK-UP
REGISTRATION FOR DIGITAL
THERMAL HALFTONE PROOFING

by

Peng-Yang Steven Chiu

B.A.Sc, The University of British Columbia, 1995

A thesis submitted in partial fulfillment of
the requirements for the degree of

Master of Applied Science

In

The Faculty of Graduate Studies

Department of Electrical and Computer Engineering

We accept this thesis as conforming to
the required standard

THE UNIVERSITY OF BRITISH COLUMBIA

November 2002

Department of Electrical & Computer Engineering

The University of British Columbia
Vancouver, Canada

Date November 20, 2002

ABSTRACT

Proofing in the printing industry is a vital process of predicting and thus reducing the costs of errors that may show up in the final prints. Digital thermal halftone proofs are produced off-press and offer dot-for-dot match to the press sheet. To produce such proofs with images on both sides of the proof sheets accurately aligned, however, is typically done with skillful manual labor to control and compensate for the thermal expansion of the images due to the step of laminating images to the paper. The alignment of the images is called backup registration. With the introduction of the second generation of thermal proofing media known as direct-to-paper, the lamination step is unnecessary, thus, it is possible to design an automatic backup registration method that can be integrated into many of the existing digital thermal proofing devices.

This thesis proposes a novel approach to automatic backup registration by detecting the orientation of the proof sheet (geometric detection), and then adjusting the images on both sides (geometric correction). The geometric detection uses the surface reflectivity differences between the proof sheet and its background to determine the edge positions of the sheet. The geometric correction shifts and rotates the images according to the detected edge positions and various other factors.

The proposed algorithm is developed and implemented on Creo Products Inc.'s Spectrum proofing device and numerous two-sided proof samples have been produced to evaluate the precision of backup registration. Since all the samples have demonstrated backup registration within the required 1mm precision and the algorithm is implemented without additional hardware, there is a high possibility of commercial application for the proposed method.

TABLE OF CONTENTS

LIST OF FIGURES

LIST OF TABLES

ACKNOWLEDGMENTS

Chapter 1

INTRODUCTION

Printing, a means of graphic communication, is the mass reproduction of visually perceivable images, typically with ink on paper. Since Johannes Gutenberg invented the use of metal cast types and screw-and-lever press for printing in 1440 A.D., the printing process depends heavily on skilled specialists performing various manual tasks in order to produce high quality publications. With the introduction of computers into the printing process, many of such tasks can be done digitally on the desktop, commonly known as desktop publishing. The digital evolution continues today with the goal of making the printing process more efficient by automation while achieving higher quality results. Despite the changes, the printing process today still consists of the same three major stages as in 1440: prepress, production, and post press.

Prepress is the process of preparing images and texts to be published in order to be ready for printing. In offset printing where a press is involved, the prepress produces proofs and plates. Proofs are used as tools to communicate the expectation of the print buyer and the capability of the printer between the two parties [1]. Once the print buyer approves the proofs, the prepress process continues on to making the plates, which are mounted on the press for mass production of the publication.

The production stage is the collection of steps required to print the copies of the publication, including make ready, press check, and production run. Make ready is the process of preparing the press for printing a particular job, such as cleaning

the press rollers from the previous job, adding ink supply to the press, making various press adjustments, and mounting the plates on the press. Once the press is ready, a few copies are printed for quality assurance in the process known as press check. These early copies are compared with the proof to ensure they meet the print buyer's expectation. Once the press check is passed, the actual production run starts.

Post press consists of various finishing operations to convert printed sheets to finished pieces. Some print jobs such as posters can be delivered as printed, but most jobs must be finished through folding, trimming, and binding due to the fact that one single press sheet often contains multiple pages of the publication. For the pages in the finished pieces to be in the proper sequences, the layout of the press sheets must be planned during prepress in an operation known as imposition.

Both the production and the post press processes depend upon the correct outputs of prepress, therefore the cost of a prepress error increases exponentially if it is detected later in the printing process [2]. As shown in Figure 1, when the prepress error is caught during press check, the cost of the error is the cost of remaking the plate and make ready. However, if the error is detected after post press, it will have cost the printer the post press process, paper and ink, production time, make ready, as well as plate remake.
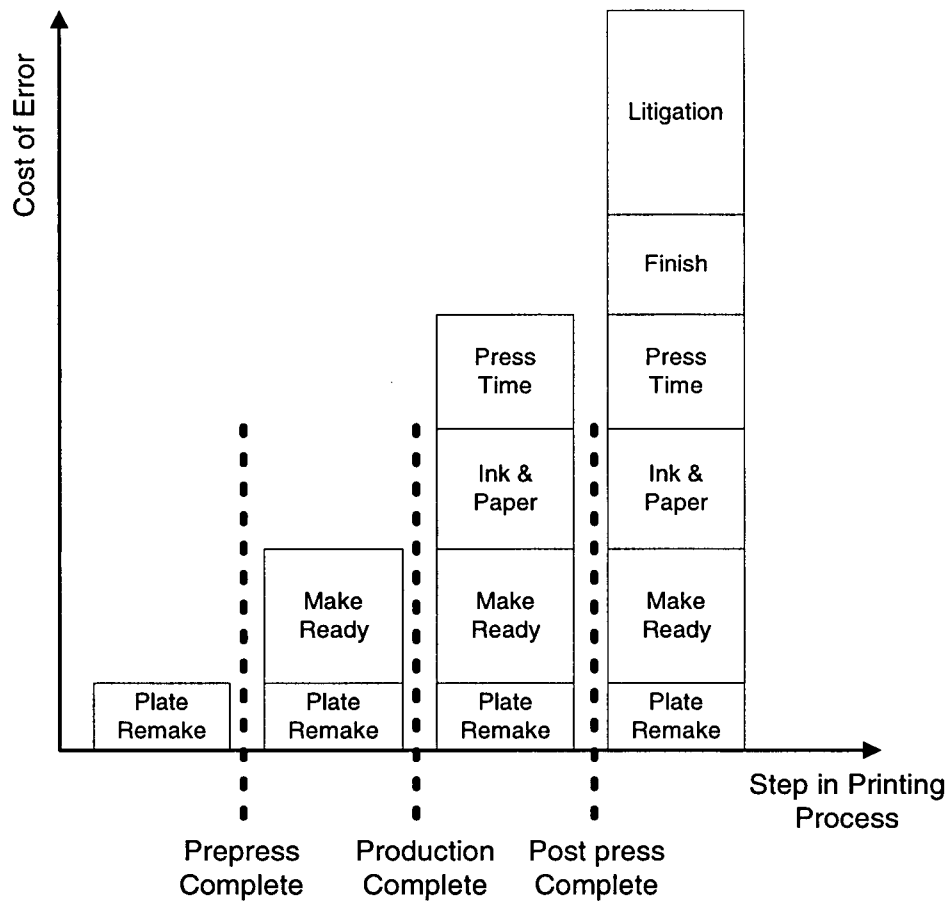
Figure 1 Cost of Prepress Errors

From the print buyer's perspective, a prepress error can cause the publication to miss the deadline if the publication has to be reprinted. Therefore, prepress proofs that match closely to the final printed product are essential to the early detection of prepress errors prior to production [3]. They are very important to both the printer and the print buyer.

Even though proofing plays a vital role to all stages of the printing process, there is still no single method to proof all aspects of the prepress output. Since most

prints are done on both sides of the paper, the front image must be properly aligned with the back image in order for the post press to fold and trim the press sheet properly. This front to back image alignment is known as backup registration. Digital thermal halftone proofs, the highest quality prepress proofs available, can match the press sheets in terms of color accuracy and half tone dot structures, but cannot match the backup registrations without delicate manual adjustments [2]. Backup registration is an important characteristic to be exhibited by proofs in order to check the imposition in the prepress as well as to demonstrate the look and feel of the final printed products like to the print buyers.

1.1   Challenges of Backup Registration

Backup registration presents a significant challenge for digital thermal proofing due to the fact that proofing images need to be laminated on to proof sheets. The heat required by lamination causes the proofing images to expand slightly. Thus, in order to laminate images on both sides of a proof sheet with backup registration, this thermal expansion effect must be kept consistent [1].

In addition to the challenge caused by lamination, automatically aligning images on both sides of the proof sheet accurately, typically within 1mm, is not an easy feat either. For proofing methods that do not require lamination, such as inkjet proofing, backup registration is achieved through the following steps:

1. Precisely load the proof sheet front side up into the imaging device to a fixed position within the required backup registration accuracy. In addition, the orientation of the loaded paper must be orthogonal to the imaging axis.

2. Image the proof and then unload the proof sheet.

4

3. Repeat step 1 and 2 for the backside with the same precision.

Proofing devices (proofers) that utilize this method need precision mechanical hardware to control the position and orientation of the paper. Due to the high cost of precision hardware, most proofers are designed such that human operators manually load and adjust the paper for backup registration in order to keep the costs of devices competitive [4].

1.2   Motivations and Objectives

Since 2001, Imation Enterprises Corporation has been developing the second generation of thermal proofing media for Creo Product's Inc.'s Spectrum digital thermal halftone proofers. This new proofing media, known as direct-to-paper (DTP), does not require lamination. Therefore, the problem caused by thermal expansion of proofing images is non-existent. With the challenges of controlling the thermal expansion due to lamination resolved by DTP, it is desirable to develop a method for low cost, automatic backup registration that can be integrated into the existing Spectrum proofers. There are more than five hundred Spectrum proofers installed worldwide, and as the automatic backup registration method shall require no additional hardware, the cost of adding the new functionality is minimized.

This thesis presents a novel approach to solving the backup registration problems by manipulating the front and back images to compensate for the differences in positions and orientations of the proof sheet. Images can be shifted and rotated accordingly such that backup registration is achieved without manual adjustment. by detecting the shifts and rotations of the proof sheet after it has been loaded in the proofer. In addition, this method does not require precision mechanical components by controlling the imaging process rather than the proof sheet

handling process. Therefore, the proposed method can be integrated into existing Spectrum devices while satisfying the requirement for no additional hardware.

The proposed method consists of two processes: geometric detection and geometric correction. The geometric detection detects the shifts and rotations of the proof sheet with respect to a known position. It is performed twice when making a two-sided proof: after the proof sheet is loaded prior to imaging the front side and also after the sheet is reloaded prior to imaging the back side. The geometric correction uses the parameters obtained by the geometric detection and adjusts the imaging algorithm to compensate for the shifts and rotations of the proof sheet. It is performed during imaging both the front and the back.

To study the feasibility of commercial applications, the consistency and accuracy of the proposed backup registration method is analyzed both empirically and statistically.

1.3   Platform Functional Requirements

Although designed for implementation on the existing Spectrum proofers, the proposed backup registration method can be adapted by any proofing platform provided that following functional requirements are met.

1. Compatibility with DTP proofing media. The Spectrum proofer is DTP capable since this proofing media is designed specifically for Spectrum.

2. A detection mechanism that can distinguish between the proof sheet and its background. The Spectrum proofer has a focus laser system for distance measurement during imaging. For the purpose of geometric detection, we designed and implemented a new firmware algorithm utilizing the focus laser system to detect the edge positions of the proof sheet.

3. Actuators to accurately move the detection mechanism to any position on and around the proof sheet so that the edges of the proof sheet can be detected. The main-scan and sub-scan actuation systems in the Spectrum proofer are controlled by a new firmware algorithm to move the focus laser into position for detecting the edge positions of the proof sheet.

4. Ability to shift the image to any location on the proof sheet accurately. This is required by geometric correction to shift the image to compensate for shifts in loading the proof sheet. The Spectrum already supports this function with the data path, main-scan actuation, and sub-scan actuation systems. Therefore, the geometric correction algorithm is used to calculate the shift parameters obtained by geometric detection and applies the results to control shifting of the image.

5. Ability to rotate the image both clockwise and counter clockwise. The amount of rotation needed depends on the amount of proof sheet rotation that may occur. For implementing geometric correction on the Spectrum, the image rotation is achieved by main-scan shearing and sub-scan shearing. Main-scan shearing is done by orthogonal correction that manipulates the image data to compensate the helical distortion during imaging. Geometric correction needs to be able to control the amount of orthogonal correction in order to get the right amount of main-scan shearing. Sub-scan shearing of the imaging data is not supported on the existing Spectrum systems thus a new algorithm needs to be designed and implemented.

6. Ability to plot the image data mirrored with respect to one of the imaging axis. Although the Spectrum has yet to support this function, it can be

implemented using the existing data path system by designing a new feature in its controlling firmware.

1.4   Organization of the Thesis

The thesis is structured as follows: Chapter 2 provides an overview of digital prepress operations and different methods of digital proofing available today. The pros and cons of each method are examined to establish the uniqueness of two-sided digital thermal halftone proofing with backup registration. Chapter 2 also explains the steps in the digital thermal proofing process and provides an overview of the Spectrum proofer. Chapter 3 represents the proposed backup registration method in mathematical formulas. Chapter 4 presents details of the algorithm using focus laser for geometric detection on proof sheets including different methods tested for improving the reliability, consistency, and accuracy. Chapter 5 looks at the algorithm used for geometric correction of the proofing images in shift correction and rotation correction. Chapter 6 examines several methods of measuring the accuracy of backup registration and the overall accuracy of the proposed method is analyzed. Lastly, Chapter 7 concludes the thesis with a summary and suggestions for future works.

Chapter 2

DIGITAL PREPRESS AND PROOFING

Proofing is the process of producing a representation of the final printed product as an intermediate step to assure quality control and accuracy in the printing industry. A proof is a reproduction of what the printed job should look like as per the client's expectation. As mentioned in Chapter 1, printers cannot afford to make a mistake during the complex process of mass-producing a print job due to the costs of paper, ink, labor, press time...etc. Therefore, proofs are used to obtain the customer's agreement on the content, the color, and the positions of images and texts on the page layout. Printers also use the proofs as references to calibrate the press to ensure the print jobs meet client's expectation. Figure 2 shows the typical printing cycle and the role of proofing. The proof is produced after the prepress process is completed, so it is important to understand the operations of prepress and the potential problems in each step. The role of proofing is to successfully predict these potential problems prior to press production.

Chapter 2 first overviews the major operations in today's digital prepress process and the potential problems that may arise in each step. Secondly, the classification and the applications of different proofing methods are discussed with emphasis on digital proofing. Lastly, this chapter looks at digital thermal proofing in detail, including the physics behind thermal imaging and including an overview of a thermal proofing device, the Spectrum proofer.
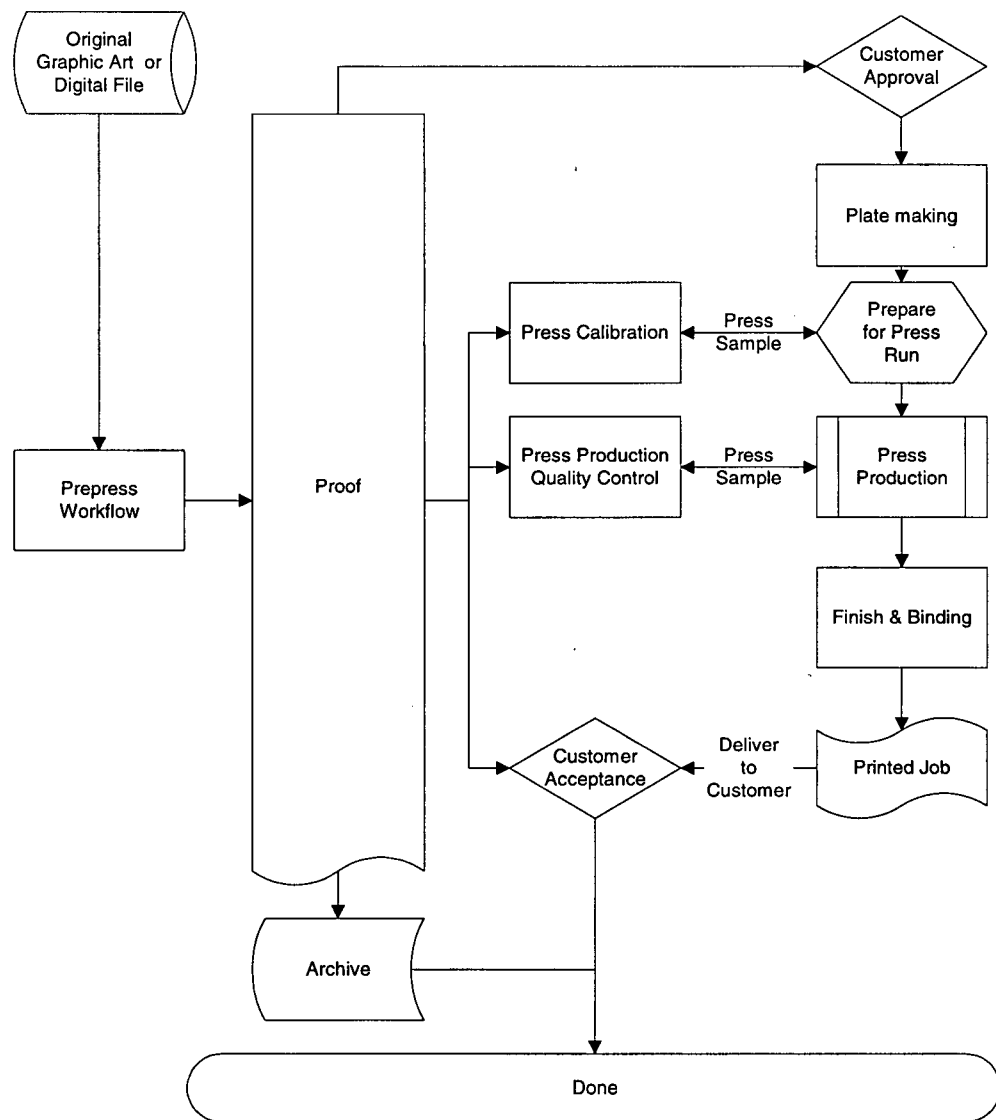
Figure 2 Printing process and Proofing

2.1 Digital Prepress

The digital prepress process involves the preparation of pages for reproduction on press. From the printer's point of view, digital prepress starts when the

customer submits the materials to be published, either in digital files or original artwork. The first step is to "normalize" the material by converting it for further processing into one single standard digital format known as a "job". The normalization operations include scanning of the original artwork, digitally touching up images, as well as file format conversion. Once the job is normalized, it will be subject to the following operations: trapping, color management, halftone screening, and imposition.

2.1.1   Trapping

Trapping and overprinting are techniques to hide the registration flaws caused by misalignment of plates or stretch of paper on the press [5]. The registration flaws are most noticeable where two colors meet. In Figure 3, object A is a lighter color than object B.
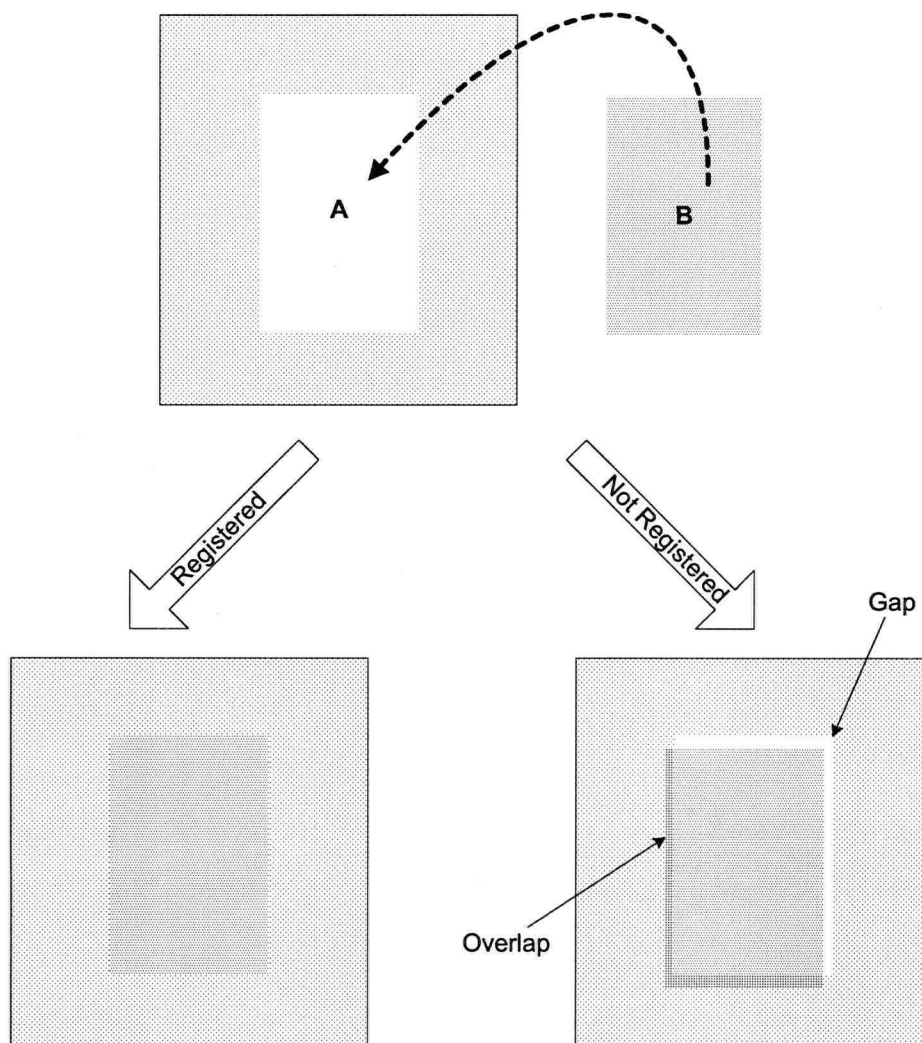
Figure 3 Gap Caused by Mis-Registration

If plates on press are registered, there is no gap between the objects. However, if mis-registration occurs during press production, the gap appears on the print. To hide the gap, object B is trapped by overprinting such that the two object overlap in the print. As shown in Figure 4, the result is a color-shifted border around object B known as a trapping artifact that is less noticeable than the gap.
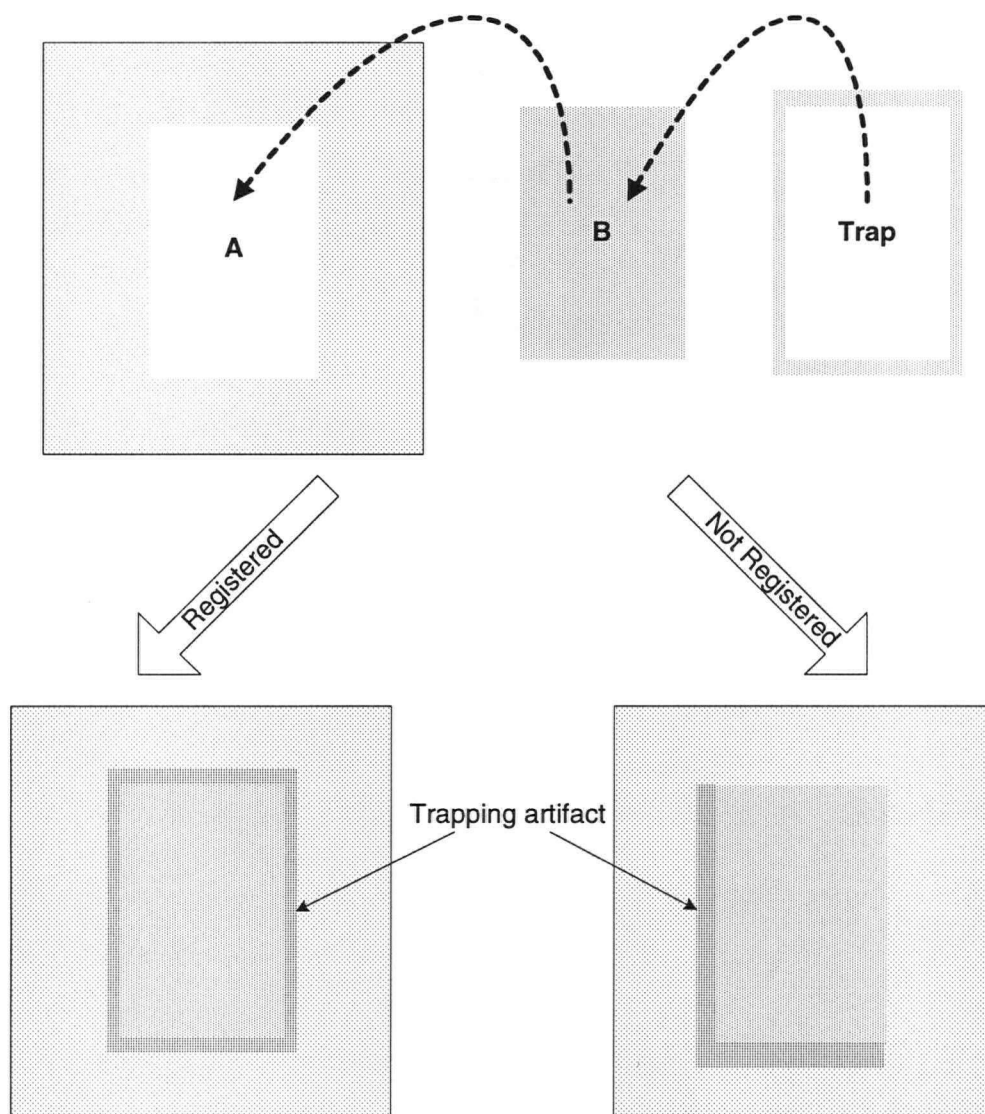
Figure 4 Trapping Artifacts

The printer needs to obtain the customer's approval on the acceptability of the trapping artifacts prior to production, so proofs need to accurately represent this artifact.

2.1.2　Halftone Screening

To represent continuous tone images with a finite number of colored inks, the images are screened as single color dots in different sizes to simulate tones of colors on press. This process is known as halftone screening. Figure 5 shows the halftone screens representing 25%, 50%, 75%, and 100% tones.

25% tone and halftone dots

50% tone and halftone dots

75% tone and halftone dots

100% tone and halftone dots
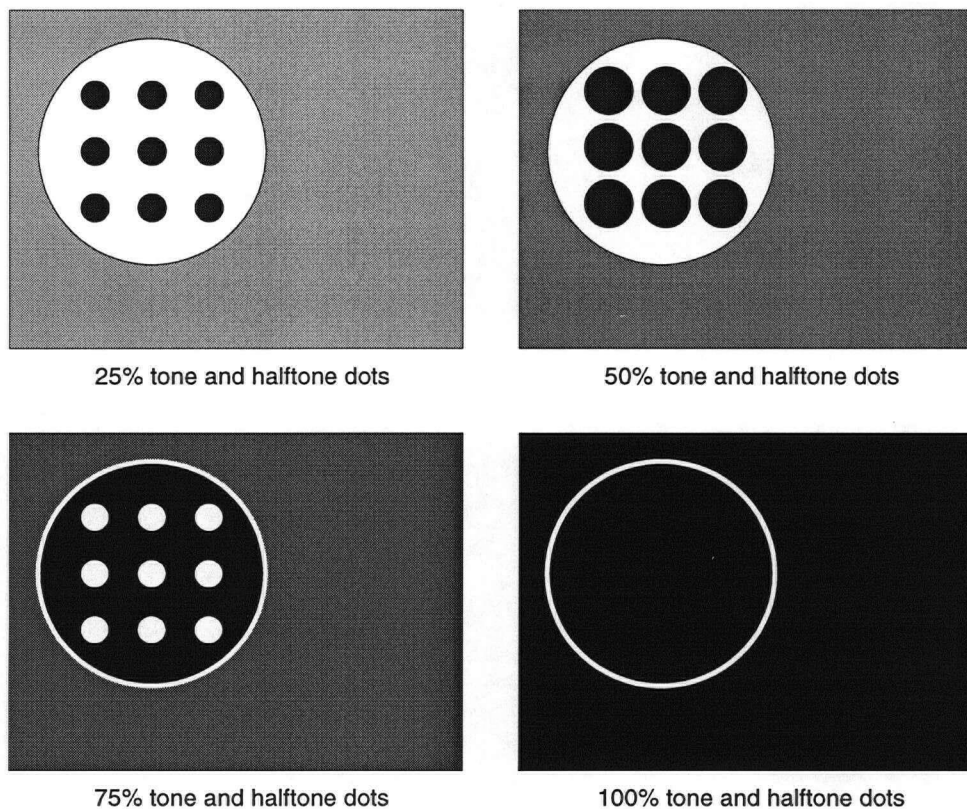
Figure 5 Halftone Screens and Magnified Dots

When two halftone screens are oriented at less than a 30-degree angle, a noticeable pattern of interference lines, called a moiré pattern, may appear [3]. The moiré pattern causes the image to appear grainy with many undesirable

artifacts. In Figure 6, when overlaying screen A on top of screen B with a 30° angle between them, the result is uniform shade throughout the image.

30° halftone screen

on

0° halftone screen

No moiré

0° halftone screen

on

0° halftone screen
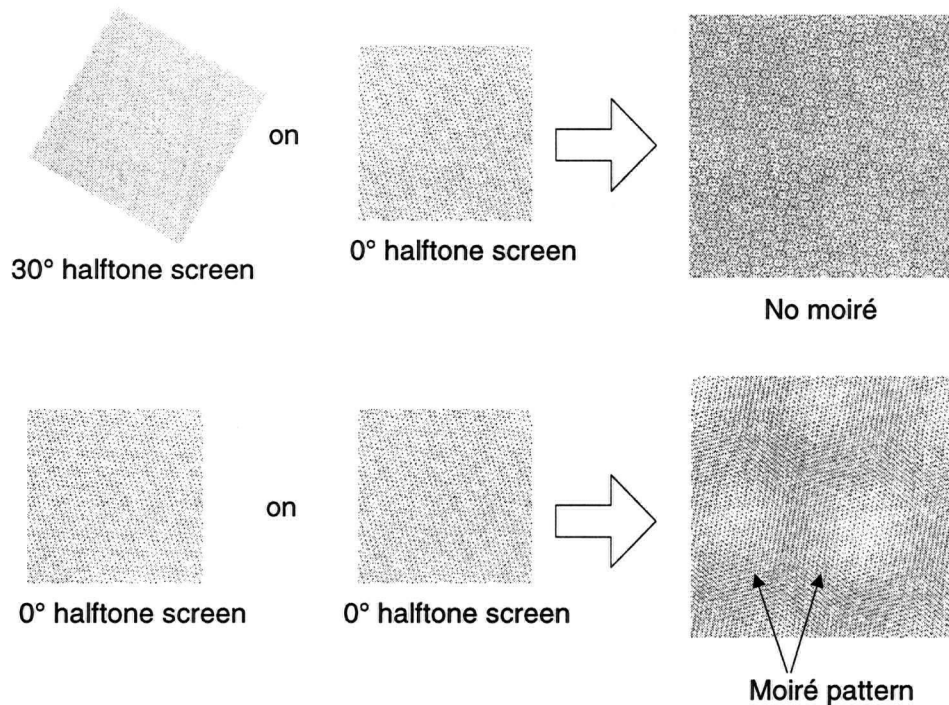
Moiré pattern

Figure 6 Screen Angles and Moiré Patterns

However, the moiré pattern appears when the angle between A and B are reduced to 0°. Since the screens consist of dot patterns at 90° to each other, only three screens can be used with at least 30° angle between each of them. In color printing, at least 4 process colors, cyan, magenta, yellow, and black, are needed to achieve a satisfactory representation of continuous tones of color. Therefore, moiré patterns are always present in any color print with halftone screens. In order to reduce the effect of moiré patterns, printers usually put yellow, the lightest in the four process colors, at an angle of 15° from cyan and magenta [1].

15

Thus, it is important for proofs to be able to accurately represent halftone dots so the moiré effect can be identified early in the printing process [2].

2.1.3   Color Management

Color management is used to correct dot gain that occurs when wet ink spreads as it is absorbed by paper. Dot-gain causes the printed dot size to be slightly larger than intended and makes the printed job to appear darker than intended. The amount of dot gain depends on many factors such as the types of ink and paper used, press settings, and the temperature and humidity during production [1]. Therefore, it is important for proofs to show accurate colors as per the customer's expectation so that color management can properly correct dot gain during prepress and production.

2.1.4   Imposition

Imposition is the process of arranging pages of a publication so that when the sheets are printed and folded for binding, the pages will be in the proper sequence. The imposition process changes depending on how the press sheets are to be folded, trimmed, and bound. Figure 7 is an example of an imposition for a 16-page publication that is to be folded with one parallel fold along line 2 and two right angle folds along line 1 and 3, trimmed along line 2, and bound along line 3.

FrontSide

C			B
P5	P12	P9	P8
P4	P13	P16	P1
D			A

Fold Line 2
Fold Line 3
Fold Line 1
Fold Line 3

3 →   1 →   3 →

2 →

2 →

BackSide

D'			A'
P3	P14	P15	P2
P6	P11	P10	P7
C'			B'
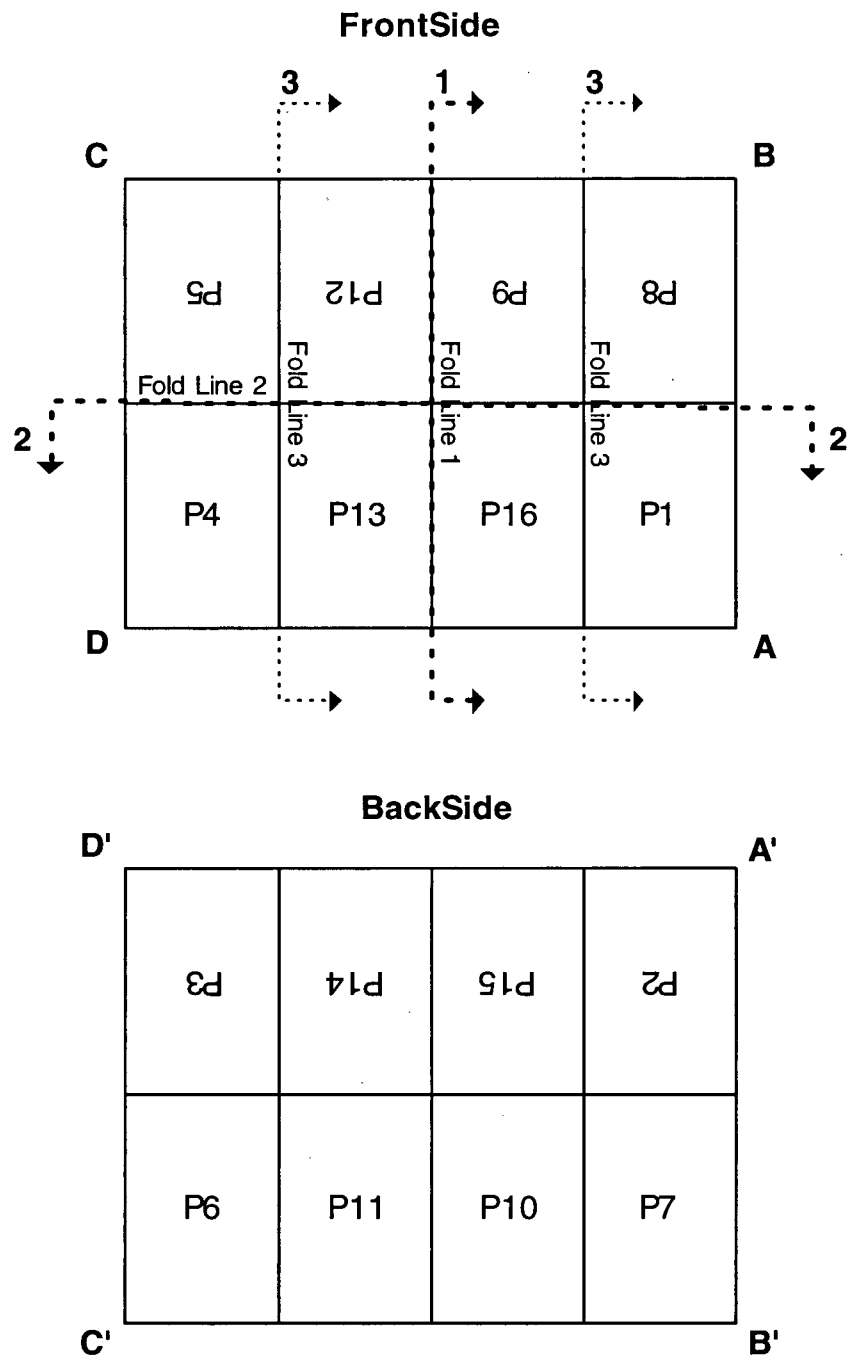
Figure 7 Imposition for a 16-page Publication

17

In this example, the sequence of fold must be done in the sequence as specified by the line number for the pages to end up in the correct sequence. Although imposition proofing software tools exists, for a specialized job, it is still necessary to produce a hard copy proof to ensure the correctness of imposition.

2.2   Methods of Proofing

The printing industry is constantly developing new methods of proofing that are faster, cheaper, and produces better quality proofs as the printing process evolves. As shown in Figure 8, proofs fall into one of the following categories based on how they are produced.
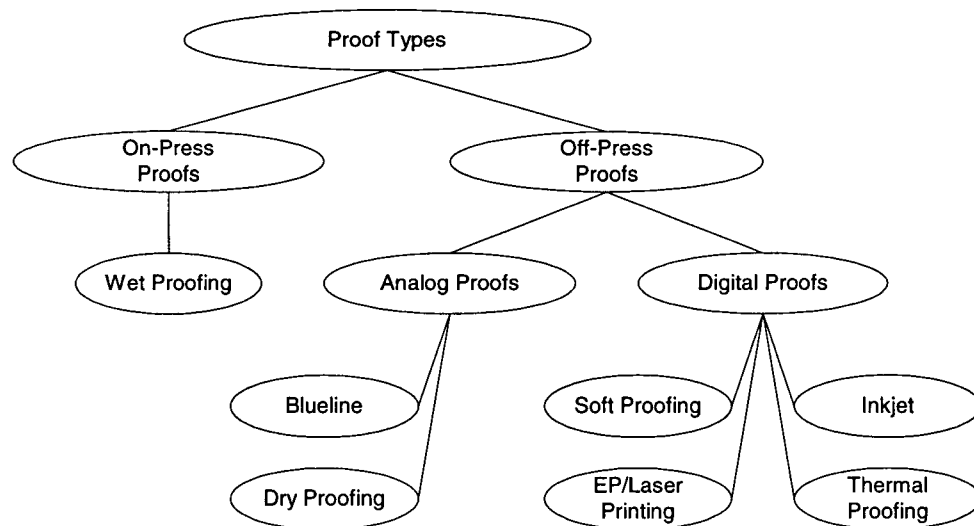
Figure 8 Methods of Proofing

Proofs can also be categorized as content proofs or contract proofs based on how they are used.

2.2.1 Content Proofs and Contract Proofs

Content proofs are a reasonable representation of the print job in terms of its content but not its color accuracy. Some content proofs also lack the same halftone dot structures of the printed piece. An example of a content proof is a blueline proof, which shows texts and pictures in single color, positioning of the textual and pictorial elements, and backup registration. However, since the blueline proof is monochrome, it does not show the colors of printed job thus cannot be used to verify if colors are what the client expected. Content proofs include soft proofs (inaccurate color representation), blueline proofs (no color), some inkjet proofs (no halftone dot structure), and proofs produced by color laser printers (inconsistent and inaccurate color) [3].

Contract proofs, on the other hand, are exact representations of the print job in both color accuracy and dot structure. They are used prior to press production to obtain the client's approval, during production to refer the printing quality to the proofs, and after production to demonstrate the printed job matches the client's expectation [4]. It is often used as a legally binding contract hence the name contract proof. Proofs that are considered contract quality include on-press proofs, analog color proofs, and digital halftone proofs. The costs of contract proofs are significantly higher than content proofs thus they are typically used when there will be long press run (10000+ copies) or high quality jobs [6]. High quality color inkjet proofs are some times accepted as contract proofs even through they do not have the same halftone dot structure as the printed pieces. Contract proofs such as digital thermal proofs are exact simulations of the press sheets, thus it can be used to verify and control the pre-press and on-press process.

2.2.2 On-Press Proofs and Off-Press Proofs

On-press proofs, as the name indicates, are produced with the same plate, paper, and inks on the same press that prints the production job. To produce the on-press proof, the printer has to setup and calibrate the press as if the real press run is going to take place. Therefore, on-press proofing is the best way to verify what the client is going to get when the job is completed. While there are benefits of an identical match between print and proof, on-press proofing is slow and expensive. It is slow because of the long make ready time and expensive because of the high capital and operational cost of the press. Therefore, on-press proofs are usually done late in the printing process to reduce the risks of last minute changes and correction [1]. Wet proofing is a form of on-press proof. Instead of using the production press to produce proofs, a smaller press called a wet press is used for the sole purpose of producing wet proofs, thus freeing the production press for production jobs.

In contrast to on-press proofs, off-press proofs are not produced by the printing press but by proofers. This allows the press to be dedicated on print production thus making the printer more efficient. Off-press proofs are more economical since they do not incur the expenses associated with producing on-press proofs. Thus, off-press proofs are typically done early in the printing process to reduce prepress errors. Off-press proofs are either produced from film as analog proofs or directly from digital files as digital proofs.

2.2.3 Dry Proofing

Dry proofing is one form of analog proofing that is produced from the same films that also used to produce the printing plates. Each film contains the image of a single color known as separation and is exposed over a sheet of receptor laminated with a clear photopolymer. Wherever light strikes the laminate material, it is hardened and will not accept toner. After exposure, the top cover sheet of

the laminate is pulled off to uncover the tonable surface. The areas that are to be toned are sticky and color powder toner is applied. This process is repeated for each separation and the result is a color proof image on the receptor. Dry proofs have been used widely since 1970s but have been steadily replaced by digital proofs since the introduction of computer-to-plate (CTP) technologies [5]. The reasons are:

1. With CTP technology, the printers no longer require films to make plates. Thus, by producing films for the sole purpose of making proof means extra costs in terms of material and labor.

2. Dry proofing is a labor-intensive procedure while digital proofing is automatic.

3. Dry proofing is sensitive to dust particles in the air especially the sticky tonable surfaces.

Despite its disadvantages, because the same film used to produce the printing plate is also used to produce the proof, dry proofing has the same dot-for-dot match to the printed piece. Therefore, dry proofs are used as contract proofs for checking the prepress results of trapping, screening, and color management. It is also possible to laminate an addition set of separations to the back of a dry proof through a labor intensive process that involves manual registration of the front and back images while controlling the lamination temperature to be consistent such that the images do not expand differently. The result is a two-sided color proof that can be used for checking imposition. Because of the complicated procedure required to produce two-sided color proof, printers usually produce blue lines for customers to check for imposition errors.

2.2.4 Blue lines

Blue lines, also known as blue prints or blueline proofs, are photographic prints made from films. They contain the images of a single separation on both sides of the proofs with backup registration. They are produced on paper with the same dimension as the press sheet, so they can be folded, trimmed, and bound for checking imposition such as ensuring the page sequences are correct. The front and back images on a blue line are typically registered within 1mm [1].

2.2.5 Soft Proofing

Soft proofs, also known as virtual proofs, use the computer monitor to represent the results of digital prepress. Since no film is required, soft proofs belong to the digital proofing category. Soft proofing is economical, fast, and uses no consumables. However, it cannot be use to verify the colors of the printed materials since the computer monitors use additive colors (RGB) while the printed materials use subtractive colors (CMYK, also known as process colors). Also, since there is no physical output, the overall quality of the print cannot be accurately assessed. Therefore, soft proofs can only be used as content proofs.

2.2.6 Laser Color Proofing

Laser proofing devices utilize the same electrophotography (EP) technology found in desktop laser printers. Instead of a single imaging unit with black toner, four or more imaging units are configured serially to print the process colors. The limitations in EP technology restricted its applications to only content proofing. These limitations include insufficient imaging resolution (up to 1200dpi) and inconsistent color production due to decay of electron on the imaging drum that attracts the toner [5]. The amount of toner transferred to the image, which determines image contrast, depends on the exact voltage of the charge on the imaging drum at the instant of transfer. Color laser proofing also belongs to the digital proofing category since no film is required.

2.2.7   Ink Jet Proofing

There are two types of ink jet proofing based on how ink is ejected onto paper – drop-on-demand (DOD) inkjet and continuous inkjet. DOD inkjet technology is used widely in the consumer desktop printer applications. Its print head ejects ink drops from an array of small nozzles to the paper. Because the trajectory of drops from any particular nozzle is influenced by factors such as nozzle wear, nozzle-to-nozzle alignment, ink pressure, nozzle blockages, etc., and the lack of mechanism to steer drops once they leave the nozzle, DOD inkjet can not achieve precise drop placement on the paper [5].

The continuous ink jet generate electrically charged drops continuously and deflect them to form the image on paper or to a gutter for recycling depending on the charge level. These proofers produce better quality proofs comparing to DOD ink jet proofers and can generate reasonable halftone dots.

With the popularity of ink jet in the consumer desktop market, this technology is advancing rapidly and many predict that it can provide true 2400dpi resolution and thus be used as contract proofs in the near future.

2.2.8   Thermal Proofing

Thermal proofing produces the highest quality of proofs in terms of resolution and color consistency. There are two types of thermal proofing: ink transfer and dye sublimination. The basic concept behind ink transfer is by placing a sheet coated with solid ink known as donor on top of the receptor sheet and seal the gap by vacuum such that the donor and the receptor are in solid contact. Beams of laser are applied to the donor and cause color pigments to heat up and detach from the donor sheet. When the laser is turned off, the color pigments cool down. Since the receptor attracts the color pigments better than the donor sheet, the color pigments are stick to the receptor during the cool down period. Dye-

sublimination process is similar to ink transfer, except dye is used instead of ink. When the laser heats the dye on the donor, dye turns into vapor and solidify on the receptor when it cools down. Because the dye vapor is more likely to spread than ink pigments, dye-sublimination proofs are usually inferior to ink transfer proofs in terms of image quality.

Both types of thermal proofs require a lamination step to transfer the plotted images from the receptor to paper. The lamination step is a disadvantage for thermal proofing because of the following reasons:

1. After lamination, a glossy film is left on the proof. If the printed job is to be done on non-glossy paper, it is impossible for the press operator to match the glossy finish of the thermal proof to the printed piece.

2. The heat used in the lamination process causes the receptor to expand. This effect would cause the image sizes to vary slightly from proof to proof depending on the temperature variation of the laminator. Thus, it is difficult to produce a two-sided proof with the lamination while maintaining accurate backup registration.

To address these shortcomings, the second generation of thermal proofing media, known as direct-to-paper (DTP) media, are developed. With DTP imaging, the receptor is eliminated from the proofing process altogether. Instead of the receptor, the donor is overlaid directly on top of the paper the print job will be using. Without the receptor, the lamination step is unnecessary, thus, the above problems are non-existent.

2.3   Spectrum Digital Thermal Proofing System Overview

The Spectrum digital thermal proofing system from Creo Products Inc. consists of the following six components: raster image processor, data path, imaging head,

main-scan actuation, sub-scan actuation, and media handler. Figure 9 is an overview of the Spectrum proofing system.
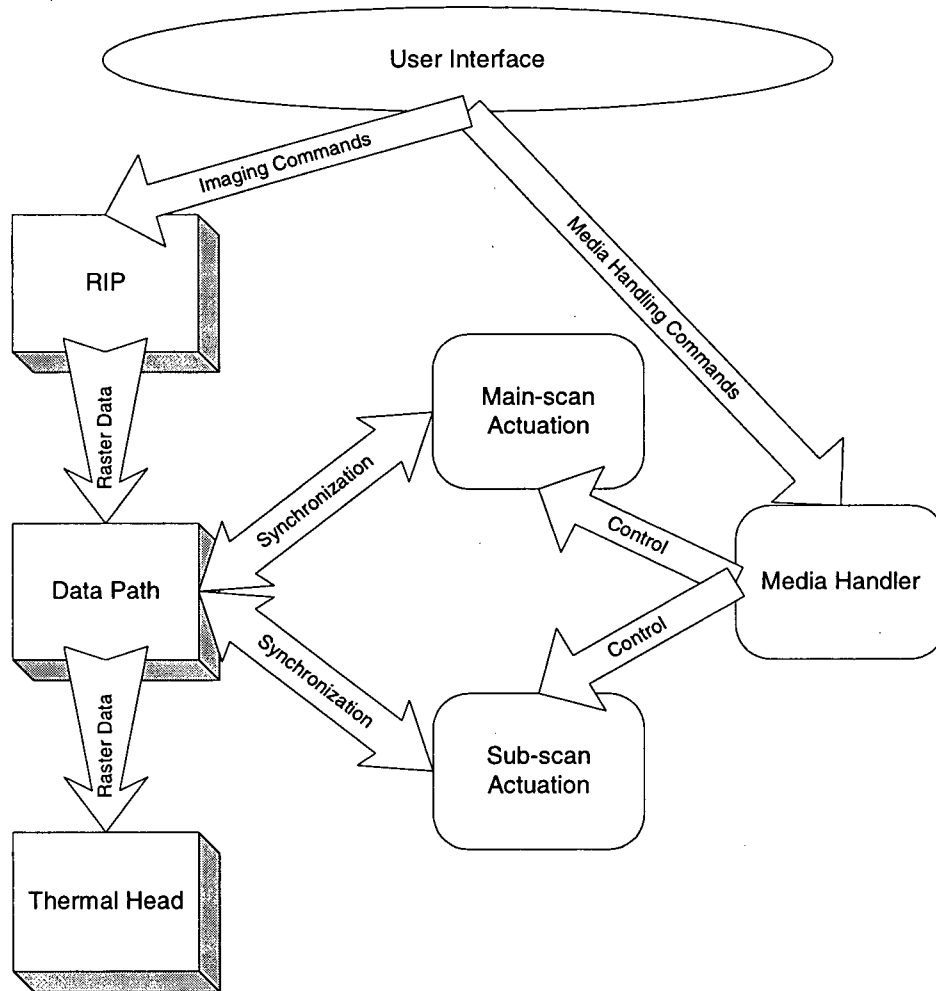
Figure 9 Components of Digital Thermal Proofing System

2.3.1   Raster Image Processor

Raster image processor (RIP) is a combination of computer hardware and software that interprets postscript files to a set of bit maps (raster data) according to a set of rules.

2.3.2 Data Path

The purpose of the data path is to receive and buffer the raster data and provide flow control such that buffer over-run and under-run caused by the difference in processing speed between the RIP and the imaging head are properly handled. In addition, the data path provides on-device data manipulation for controlling shifts and the orthogonality of the image.

2.3.3 Imaging Head

The imaging head controls the laser beams that write pixels onto the media. The beams are switched on or off according to the raster data. In addition, a focus system is used to ensure the beams are properly focused on the media to compensate for some minor variations in the distance between the head and the media.

2.3.4 Media Handler

The media handler loads the media into the device prior to imaging and unloads the media out of the device after imaging. It coordinates the main-scan and sub-scan actuation to achieve the media load and unload sequence. Figure 10 shows these sequences in the proofing process on Spectrum.

```
              ┌──────────┐
              │   Load   │
              │ Carrier  │
              └──────────┘
                   │
                   ▼
              ┌──────────┐
              │   Load   │
              │ Receiver │
              └──────────┘
                   │
                   ▼
              ┌──────────┐
    ┌────────▶│   Load   │
    │         │  Donor   │
    │         └──────────┘
    │              │
    │              ▼
    │         ╭──────────╮
    │         │   Plot   │
Repeat for all │  Raster  │
seperations    │   Data   │
    │         ╰──────────╯
    │              │
    │              ▼
    │         ┌──────────┐
    │         │  Unload  │
    └─────────│  Donor   │
              └──────────┘
                   │
                   ▼
              ┌──────────┐
              │  Unload  │
              │ Receiver │
              └──────────┘
                   │
                   ▼
              ┌──────────┐
              │  Unload  │
              │ Carrier  │
              └──────────┘
```
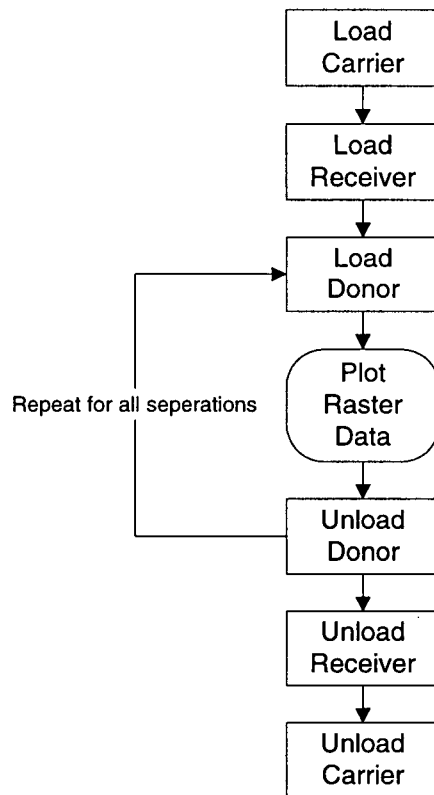
Figure 10 Spectrum Proofing Process

As discussed earlier, digital thermal proofing requires the donor and the proof sheet in solid contact in order for ink pigments to transfer from the donor to the proof sheet. In Spectrum, air is pumped out from inside the drum to create airflows through the vacuum holes on the surface of the drum, as shown in Figure 11.

27

Imaging Laser Beams

Border Tape — **Donor** — Border Tape
Proof Sheet
Donor Vacuum Holes   Donor Vacuum Holes
Carrier

Receiver Vacuum Holes

Airflows   **Drum**   Airflows
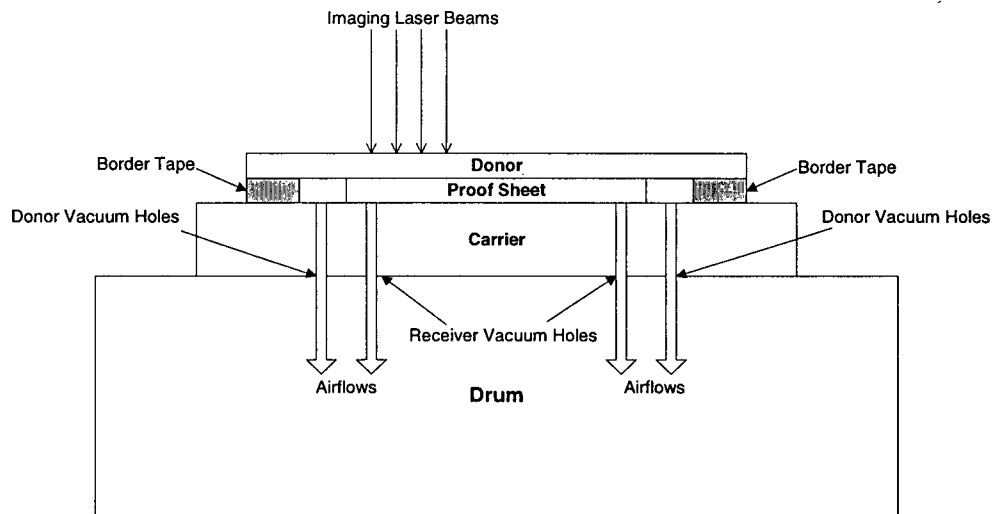
Figure 11 Cross Section View of Spectrum Proofing Media on drum

Carriers are used as templates to allow air to flow through to seal the proof sheet on the carrier and the donor on the proof sheet. Carriers are held on the drum by sets of clamps. The border tape is for propping up the edges of the donor to keep it flat while maintaining the vacuum seal between the proof sheet and the donor.

2.3.5   Main-scan Actuation

Main-scan is the direction parallel with the imaging swath or perpendicular to the channels of laser beams as shown in Figure 12.
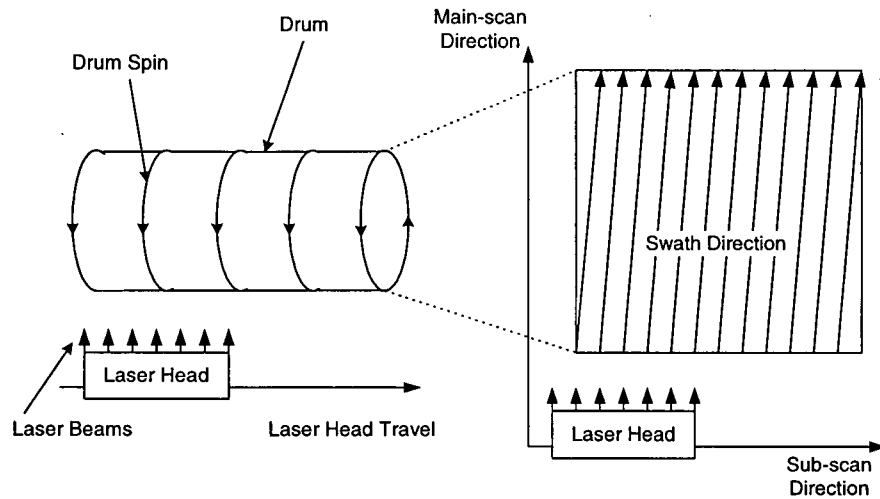
Figure 12 Main-scan and Sub-scan Directions

The main-scan actuation moves the media such that the imaging can occur in the main-scan direction. On Spectrum, the main-scan actuation is achieved by rotating a cylindrical drum with the media loaded on its surface. The rotation is a controlled motion with a servo system consists of a DC motor and an optical quadrature encoder with index pulse. It is capable of moving the drum to within 314 micro radians (μRad) or 45 μm of the specified target position.

2.3.6 Sub-scan Actuation

The sub-scan direction is perpendicular to the main-scan direction. The sub-scan actuation moves the head such that the imaging can occur in the sub-scan direction. On Spectrum, the sub-scan actuation is achieved by using a stepper motor to rotate a lead screw that the head sits on. Unlike the ink jet printers where both the main-scan and sub-scan motions are discrete, on thermal proofers, these motions are continuous. This is due to the weight of the thermal imaging head, which is substantially heavier than the ink-jet one. Hence, the frequent stops and starts of the discrete motions mean huge changes in

momentum, thus motors with high torque are needed to handle the load reliably. In addition, the continuous motion provides better image quality and higher throughput than discrete motions. The sub-scan actuation on Spectrum is capable of moving the laser head to within 1 μm of the specified target position.

Chapter 3

AUTOMATIC BACKUP REGISTRATION

Backup registration is used to align the image on the front side of the paper with the image on the backside. Most proofers achieve backup registration by loading the paper to the exact same location every time accurately [1]. This mechanical registration method requires a media handling system with precision mechanics in order to meet the accuracy requirement. On the other hand, by using the optical sensors on a proofer to detect the shifts and rotations of the loaded proof sheet, backup registration can be done by shifting and rotating the images on the both sides according to the detected orientations of the proof sheet. With this approach, there is no need for developing and building a precise media handler thus no additional hardware is needed. Thus, this optical backup registration method can be retrofitted to existing Spectrum proofers by upgrading its control software. In addition, the tolerance to variation in paper's orientation in optical registration means that simple media handler mechanics can be utilized to improve its reliability due to the reduction of precision parts. The proposed process is shown in Figure 13.
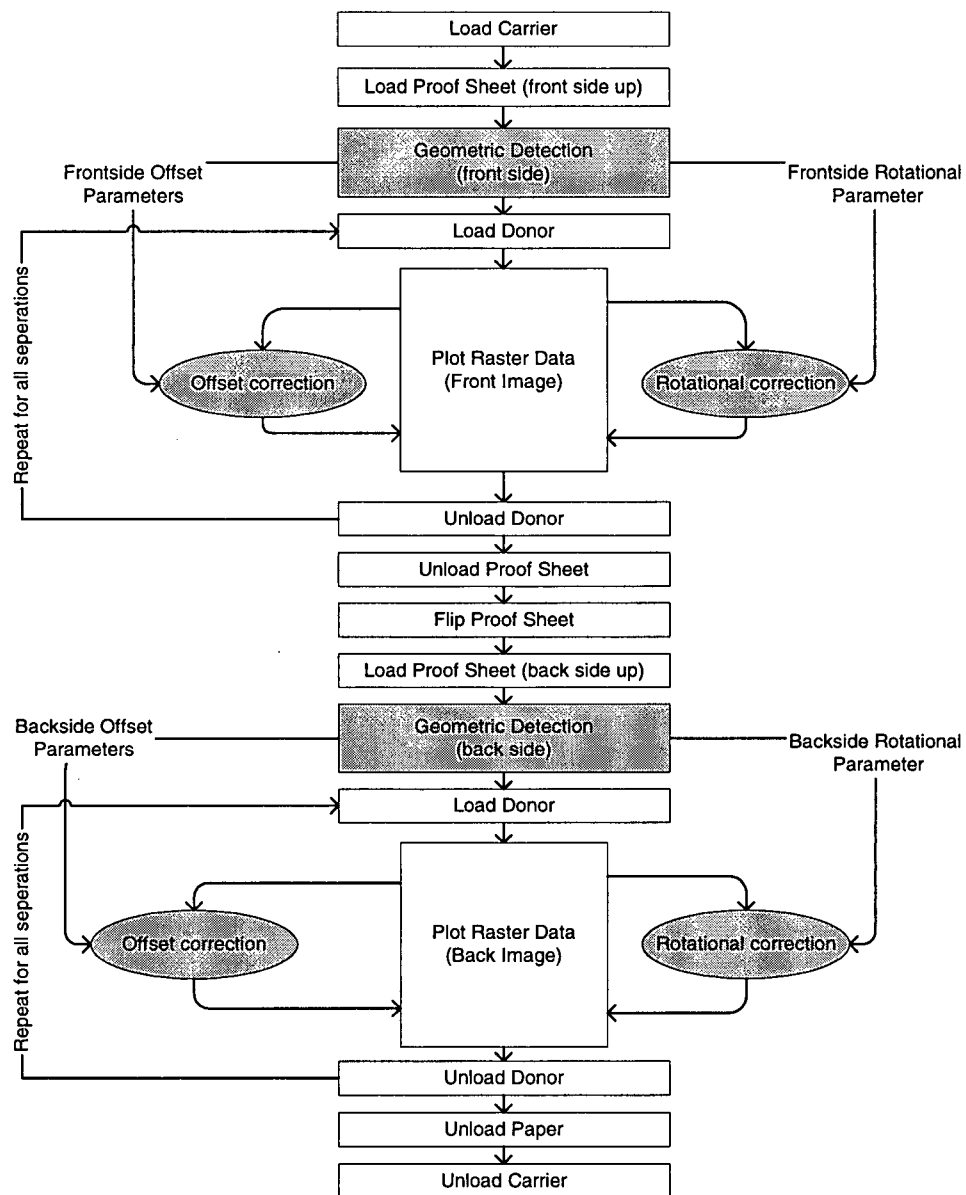
Figure 13 Two-sided Digital proofing processes

The shaded boxes in Figure 13 indicate functions that need to be designed and implemented specifically for the purpose of backup registration on Spectrum proofers.

3.1 Requirements and Specifications

The following are the tolerance requirements, precision requirements, and other specifications for backup registration in two-sided proofs. The proof sheet used has the following specifications:

- The length of the proof sheet is within 2 mm of the specified length.

- The width of the proof sheet is within 2 mm of the specified width.

- The squareness of the proof sheet is bound by its length and width specifications.

The backup registration algorithm shall be able to compensate the following variations due to Spectrum's media handling:

- From front to backside, the main-scan shift of the proof sheet shall be less than 15 mm with respect to a reference point on the carrier.

- From front to backside, the sub-scan shift of the proof sheet shall be less than 15 mm with respect to a reference point on the carrier.

- Rotation of the proof sheet shall be less than 8000µRad with respect to the sub-scan direction

- Supported media size is 22" by 30".

The optical backup registration algorithm shall achieve the same specification as blue line proofs, that is:

- All points on the front side image shall align with the backside image within 1 mm [1].

3.2 Mathematic Model

Assuming ABCD in Figure 14 is a near rectangular proof sheet and have the following properties:

$$\left\| \overline{AD} - \overline{BC} \right\| \leq 2 \text{ (mm)}$$

and

$$\left\| \overline{AB} - \overline{DC} \right\| \leq 2 \text{ (mm)}.$$

Also, $\angle A$, $\angle B$, $\angle C$, and $\angle D$ are all approximately $\dfrac{\pi}{2}$.

A rectangular raster image $I_0 I_1 I_2 I_3$ to be plotted on one side of the paper with the following equation:

$$\overline{I_0 I_1} \; / / \; \overline{AD} \hspace{4cm} \text{Equation 1}$$

By plotting $I_0 I_1 I_2 I_3$ in parallel with $\overline{AD}$, the amount of image rotation needed to achieve backup registration is reduced if the back image is also plotted in the same manner.
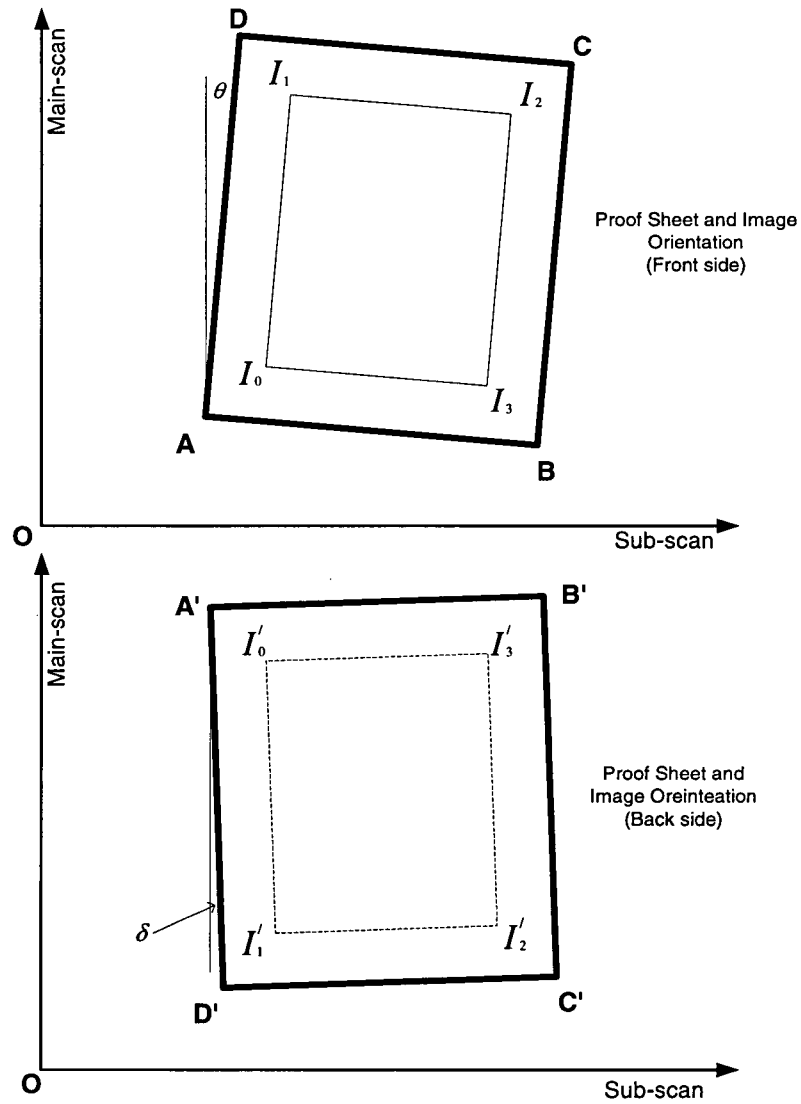
Figure 14 Orientations of Proof Sheet and Images

Other properties of the image include:

$$|I_0 I_1| = |I_2 I_3| = L \qquad\qquad \text{Equation 2}$$

35

where L is the known length of the raster image in *mm* and

$$\left|I_0 I_3\right| = \left|I_1 I_2\right| = K \qquad\qquad \text{Equation 3}$$

where K is the known width of the raster image in *mm*. In addition, the image origin I_0 can be expressed in term of the reference point of the paper by:

$$I_0 = A + \vec{w} \qquad\qquad \text{Equation 4}$$

where $\vec{w}$ is a pre-determined image offset vector in terms of main and sub-scan direction. The offset is needed to place the image on anywhere on the proof sheet.

When the proof sheet is loaded into the proofing device, the media handler applies the following operations to its orientation with respect to O, the origin of the imaging system:

1. Main-scan shift Δ_m where $\left|\Delta_m\right| \leq 15\,mm$,

2. Sub-scan shift Δ_s where $\left|\Delta_s\right| \leq 15\,mm$,

3. Rotation angle θ where $\left|\theta\right| \leq 8000\,\mu Rad$.

To plot $I_0 I_1 I_2 I_3$ according to Equation 1, the exact location of the reference point A with respect to O and the rotation angle θ must be measured by the geometric detection. In other words, in addition to the rotation angle θ, the main-scan offset Δ_m and sub-scan offset Δ_s need to be measured since:

$$A = \Delta_s \vec{i} + \Delta_m \vec{j} \qquad\qquad \text{Equation 5}$$

where $\vec{i}$ and $\vec{j}$ are the unit vector in the sub and main-scan respectively.

Once A and θ are known, the image start point I_0 can be calculated from:

$$I_0 = A + R_\theta \vec{w} \qquad\qquad \text{Equation 6}$$

where

$$R_\theta = \begin{bmatrix} \cos\theta & -\sin\theta \\ \sin\theta & \cos\theta \end{bmatrix} \qquad\qquad \text{Equation 7}$$

Since $\cos\theta = \dfrac{\overline{DA} \cdot \vec{j}}{\left|\overline{DA}\right|}$ and $\sin\theta = \dfrac{\overline{DA} \cdot \vec{i}}{\left|\overline{DA}\right|}$, once the position D is determined,

there is no need to find out the value of θ [7]. Assuming P_1 and P_2 are two

points on $\overline{DA}$, the above can also be expressed as $\cos\theta = \dfrac{\overline{P_1 P_2} \cdot \vec{j}}{\left|\overline{P_1 P_2}\right|}$ and

$\sin\theta = \dfrac{\overline{P_1 P_2} \cdot \vec{i}}{\left|\overline{P_1 P_2}\right|}$.

From I_0, any points on the image can be obtained from:

$$I_{xy} = I_0 + R_\theta \vec{t} \qquad\qquad \text{Equation 8}$$

where

$$\vec{t} = x \cdot \vec{i} + y \cdot \vec{j} \qquad\qquad \text{Equation 9}$$

where x and y are the indexes to the raster data in the sub and main-scan respectively.

Based on Equation 8, $I_0 I_1 I_2 I_3$ can be plotted on the front side of the proof sheet following Equation 1 by rotation correction.

Once the front side image $I_0 I_1 I_2 I_3$ is completed, the proof sheet is unloaded, flip around $\overline{AB}$, and loaded back into the machine. The unload, flip, and load steps apply the following operations to the orientation of the back side of the proof sheet with respect to O, the origin of the imaging system:

1. Main-scan shift Δ'_m where $\left| \Delta'_m \right| \leq 15\, mm,$

2. Sub-scan shift Δ'_s where $\left| \Delta'_s \right| \leq 15\, mm,$

3. Rotation angle δ where $\left| \delta \right| \leq 8000\, \mu Rad,$

4. Flip operation R_f where $R_f = \begin{bmatrix} 1 & 0 \\ 0 & -1 \end{bmatrix}.$

To ensure backup registration, the new location of the front image, $I'_0 I'_1 I'_2 I'_3$, after the above operations, need to be calculated by obtaining the new image start point I'_0 where:

$$I'_0 = A' + R_\delta R_f \bar{w} \qquad\qquad \text{Equation 10}$$

and

$$R_\delta R_f = \begin{bmatrix} \cos\delta & -\sin\delta \\ \sin\delta & -\cos\delta \end{bmatrix} \qquad \text{Equation 11}$$

Similar to the front side, since $\cos\delta = \dfrac{\overline{D'A'} \cdot \vec{j}}{\left|\overline{D'A'}\right|}$ and $\sin\delta = \dfrac{\overline{D'A'} \cdot \vec{i}}{\left|\overline{D'A'}\right|}$, the

positions A' and D', or any two points P_1' and P_2' on $\overline{D'A'}$, need to be measured during the backside media detection process to calculate

$\cos\delta = \dfrac{\overline{P_1'P_2'} \cdot \vec{j}}{\left|\overline{P_1'P_2'}\right|}$ and $\sin\delta = \dfrac{\overline{P_1'P_2'} \cdot \vec{i}}{\left|\overline{P_1'P_2'}\right|}$.

From I_0', any points on the new image orientation can be obtained from:

$$I_{xy}' = I_0' + R_\delta R_f \vec{t} \qquad \text{Equation 12}$$

where

$$\vec{t} = x \cdot \vec{i} + y \cdot \vec{j} \qquad \text{Equation 13}$$

To keep the imaging algorithm consistent between front and back images such that imaging always starts from the lower left corner, I_1' shall be used as the backside image start point instead of I_0'. Therefore, it is desirable to calculate I_{xy}' with respect to I_1'.

Since $I_1' = I_0' + R_\delta R_f (L \cdot \vec{j})$ (Equation 14), substituting this into Equation 12 above yields:

$$I_{xy}' = I_1' - R_\delta R_f (L \cdot \vec{j}) + R_\delta R_f \vec{t} = I_1' + R_\delta R_f (\vec{t} - L \cdot \vec{j}) \qquad \text{Equation 15}$$

In addition, I_1' cab be expressed in terms of A' and $\bar{w}$ by substituting Equation 10 into Equation 16 as:

$$I_1' = A' + R_\delta R_f \bar{w} + R_\delta R_f (L \cdot \bar{j}) = A' + R_\delta R_f (\bar{w} + L \cdot \bar{j}) \qquad \text{Equation 16}$$

In summary, the geometric detection process needs to obtain the positions of A and A', as well as detect two points on $\overline{AD}$ for the front side and two points on $\overline{A'D'}$ for the backside to calculate I_0, I_0', $\cos\theta$, $\sin\theta$, $\cos\delta$, and $\sin\delta$.

3.3 Measurements for Geometric Detection

To detect and calculate the required front and backside parameters, 4 measurements points and on the front side and 4 measurement points on the backside are needed as shown in Figure 15. Since $\overline{AD}$ and $\overline{A'D'}$ are known as main-scan edges, M_1, M_2, M_1', and M_2' are referred to as main-scan edge detection points. Similarly, M_3, M_4, M_3', and M_4' are referred to as sub-scan edge detection points because $\overline{AB}$ and $\overline{A'B'}$ are known as sub-scan edges.
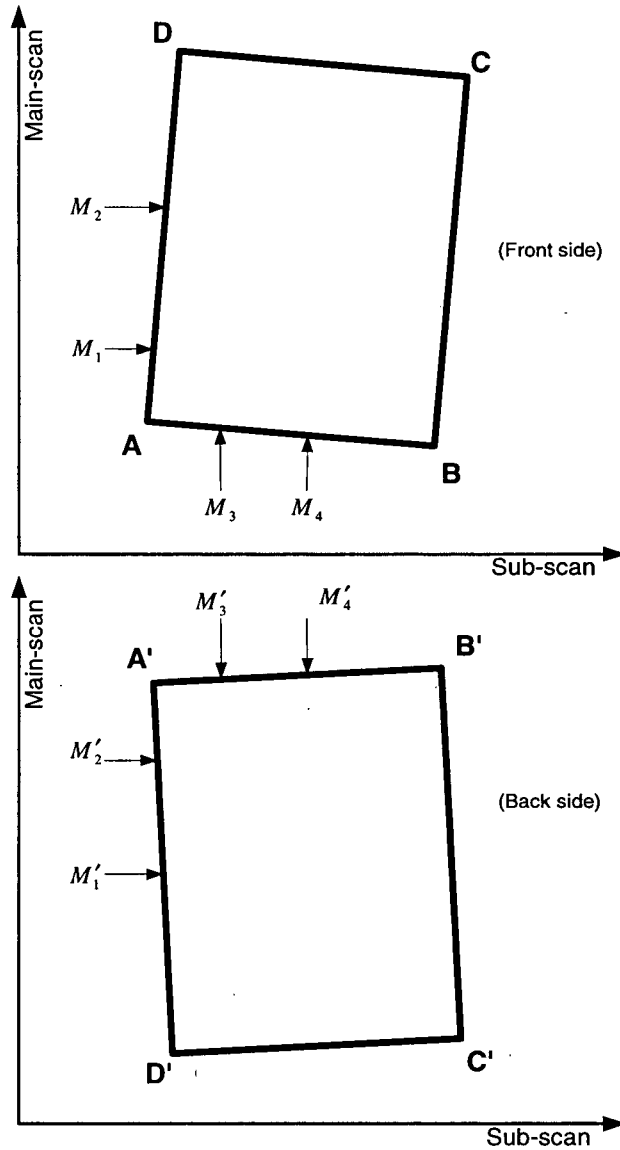
Figure 15 Measurements for Geometric Detection

By obtaining the 4 measuring points, $M_1(m_1, s_1)$, $M_2(m_2, s_2)$, $M_3(m_3, s_3)$, and $M_4(m_4, s_4)$, the exact coordinates of $A(m_A, s_A)$ can be solved by the following formula:

41

$$m_A = \frac{bf - ce}{bd - ae}$$ Equation 17

$$s_A = \frac{cd - af}{bd - ae}$$ Equation 18

where

$$a = s_2 - s_1, \ b = m_1 - m_2, c = m_1 s_2 - m_2 s_1$$

and

$$d = s_4 - s_3, \ e = m_3 - m_4, \ f = m_3 s_4 - m_4 s_3$$

Note that m_x represents the coordinate in the main-scan direction and s_y represents the coordinate in the sub-scan direction.

The following formulas are used to calculate the rotation of the proof sheet, namely $\cos \theta$ and $\sin \theta$:

$$\cos \theta = \frac{\overline{M_2 M_1} \cdot \vec{j}}{\left| \overline{M_2 M_1} \right|}$$ Equation 19

$$\sin \theta = \frac{\overline{M_2 M_1} \cdot \vec{i}}{\left| \overline{M_2 M_1} \right|}$$ Equation 20

Similarly, to obtain the required backside parameters, $M_1'(m_1', s_1')$, $M_2'(m_2', s_2')$, $M_3'(m_3', s_3')$, and $M_4'(m_4', s_4')$ are measured and the exact coordinates of $A'(m_A', s_A')$ can be derived from Equation 17 and Equation 18. Furthermore, $\cos \delta$, and $\sin \delta$ can be derived by:

$$\cos\delta = \frac{\overline{M_1'M_2'} \cdot \vec{j}}{\left|\overline{M_1'M_2'}\right|}$$

Equation 21

$$\sin\delta = \frac{\overline{M_1'M_2'} \cdot \vec{i}}{\left|\overline{M_1'M_2'}\right|}$$

Equation 22

Chapter 4

GEOMETRIC DETECTION

The geometric detection algorithm consists of two operations: main-scan edge detection and sub-scan edge detection. The purpose of main-scan edge detection is to obtain two measurement points, namely M_1 and M_2 for the front and M_1' and M_2' for the back, along the main-scan edges. Similarly, the purpose of the sub-scan edge detection is to obtain two measurement points, namely M_3 and M_4 for the front and M_3' and M_4' for the back, along the sub-scan edges. The measurement points are to be used by geometric correction to shift and rotate the images to achieve backup registration. To incorporate the geometric detection into the Spectrum proofing device economically, it must be implemented without requiring additional hardware components, such that any existing device can be upgraded easily. The no-additional hardware requirement also means that the algorithm shall require minimal computing resources so the existing micro controllers in the device can be utilized without being overloaded.

This chapter discusses the use of the focus laser system on the Spectrum proofer to detect the geometric orientation of the proof sheet on the drum. A threshold comparison scheme determines whether the focus laser is reflected by the carrier (as on-carrier signal) or by the proof sheet (as on-paper signal). The on-carrier signal profile and the on-paper signal profile are examined in detail and several methods to improve the profiles are investigated to ensure the measurement points can be detected reliably. When the proof sheet is held on the carrier by vacuum, its main-scan edges do not exhibit the same physical characteristics as its

sub-scan edges. Thus, the signal profiles near these edges also differ and can introduce inaccuracy into the measurements. A method of compensation for the error is discussed.

Finally, this chapter looks at the implementation of our algorithm and discusses the test results in terms of accuracy and repeatability.

4.1   Focus Laser System Overview

Auto focus is an essential part of the thermal proofing imaging system since the write laser must be kept focused on the media to ensure optimal amount of thermal energy is transferred. The auto focus mechanism can detect small variation in the distance between the thermal head and the media, thus adjustments can be made in the write laser's optical lenses to properly focus the laser beams. In Spectrum, the auto focus mechanism consists of a class III red laser and a detector connected to an A/D converter on the head controller as shown in Figure 16.
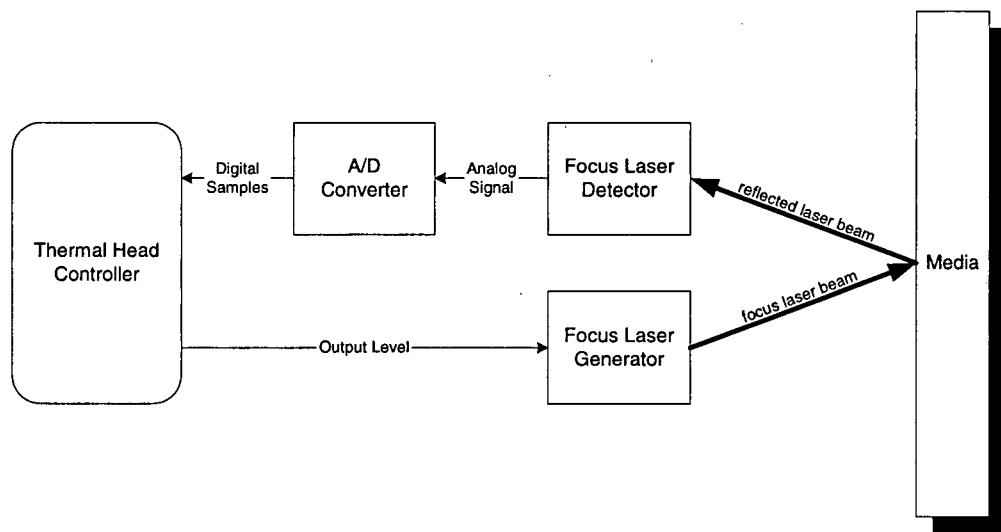
Figure 16 Focus Laser System Overview

The thermal head controller can turn the focus laser generator on and shoot a beam of laser on the media. The media reflects a portion of the laser beam back to the focus laser detector that converts light into the analog signal that feds into the A/D converter. It samples and converts the analog signal to digital values for the thermal head controller to read. Thus, if the media is highly reflective, the head controller reads large values. In contrast, if the media absorbs light or deflect it away from the detector, the head controller reads small values. This behavior is the basis of the edge detection algorithm.

4.2   Edge Detection Algorithm

By moving the focus laser across the transition between the carrier and the proof sheet while sampling the reflected focus laser light level in the detector, the exact position of the transition can be isolated when the light level crosses the threshold. As shown in Figure 17, by comparing light levels sampled with a pre-defined threshold, whenever the light level reading switch from below to above the threshold, the edge position is found.
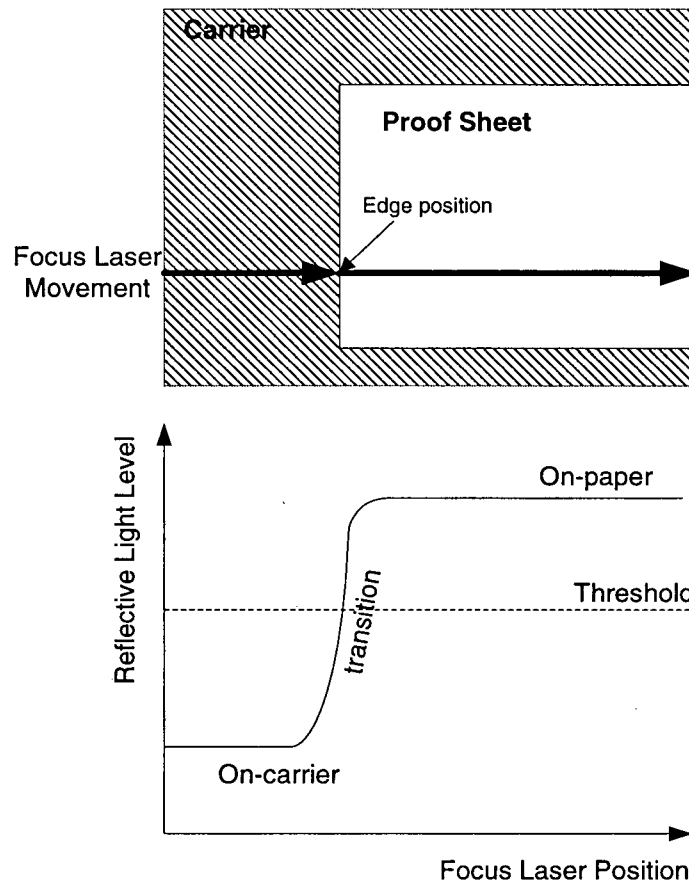
Figure 17 Edge Detection Algorithm

The advantage of this algorithm is in its simplicity. The only real time operations are sampling the light level and comparing the samples with the threshold. This means that it can be done in real-time with limited computing resources such as in the head controller. On the other hand, this method needs the difference between low light level and high light level to be large enough such that the threshold can be chosen with minimal false edge detection. In addition, the transition from on-carrier to on-paper must be sharp for accurate detection of edge positions.

4.3   Profiles of On-carrier and On-paper Signals

To obtain the signal profile of certain surface, N readings of the reflected light level are sampled at random positions on that surface while the power output of the focus laser generator is held at a fixed level. Figure 18 shows the samples of the signal strength of reflected light on bare carrier and on paper with 100% of laser power output.
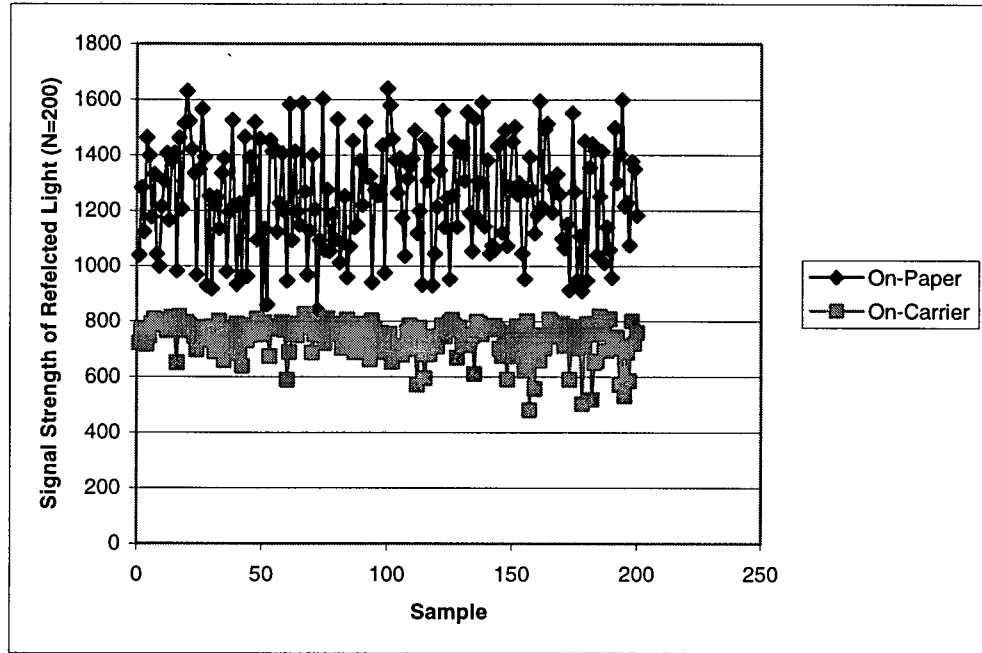
Figure 18 Samples of On-Carrier and On-Paper Signals

To study the laser reflective properties (surface reflectivity) of these two surfaces, statistical distribution of samples is graphed. Figure 19 shows the distribution of the samples for the carrier and the proof sheet with focus laser at 100% power level.
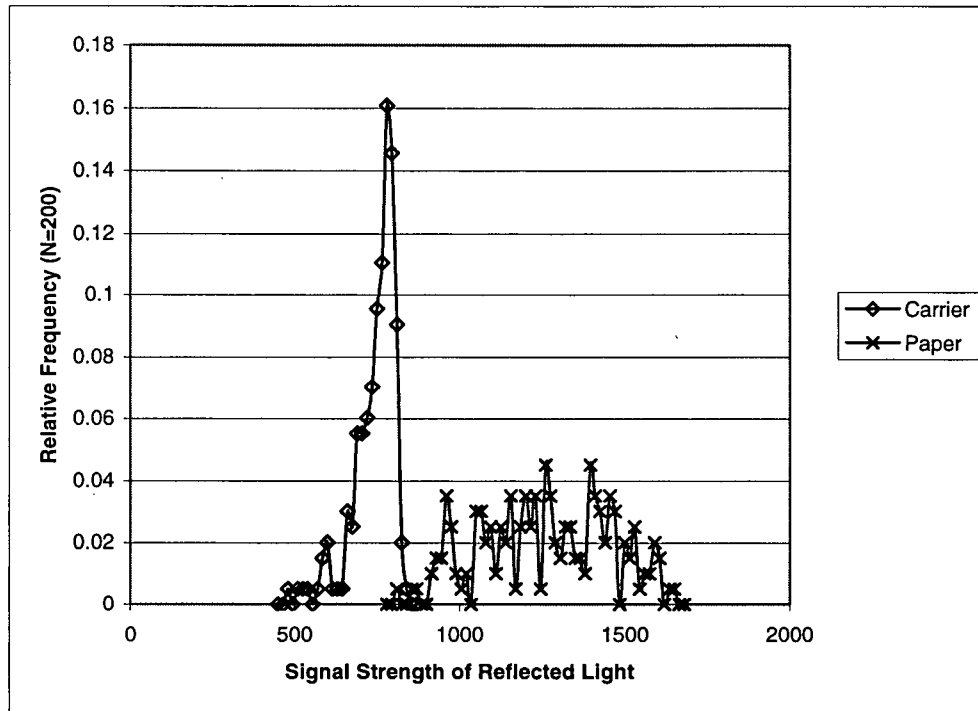
Figure 19 Relative Frequency of On-carrier and On-paper Signal Strength

As shown in Figure 19, the surface of the proof sheet is more reflective than the carrier since the on-paper signal is generally stronger than the on-carrier signal. This is due to the color of the surfaces: the white proof sheet is more reflective than the black carrier. In addition, since the surface of proof sheet is not smooth, when the focus laser hits it, the reflected light level varies over a wide range due to the diffusing effect. On the other hand, the carrier surface is a smooth one. Therefore, the reflected light level on carrier does not deviate much from its mean.

As previously mentioned, to detect the edge reliably, the on-carrier signal must be significantly lower than the on-paper signal. However, Figure 19 shows that there is an overlapping region between the on-carrier and on-paper signal profiles.

Therefore, it is impossible to establish a threshold to reliably distinguish between the two signals unless either the on-carrier signal is lowered or the on-paper signal is raised. Since the output of the focus laser is already maximized, it is unlikely that the on-paper signal can be raised any further. Thus, the solution to this problem lies in the lowering of the on-carrier signal.

4.4 On-Carrier Signal Profiles Improvement

To lower the on-carrier signal, the amount of reflected laser entering the focus laser detector must be reduced. There are two means of achieving this: by deflecting the light away from the detector (diffusion) or absorbing the focus laser on the surface so no light is reflected (absorption). The diffusion and absorption are graphically represented in Figure 20.
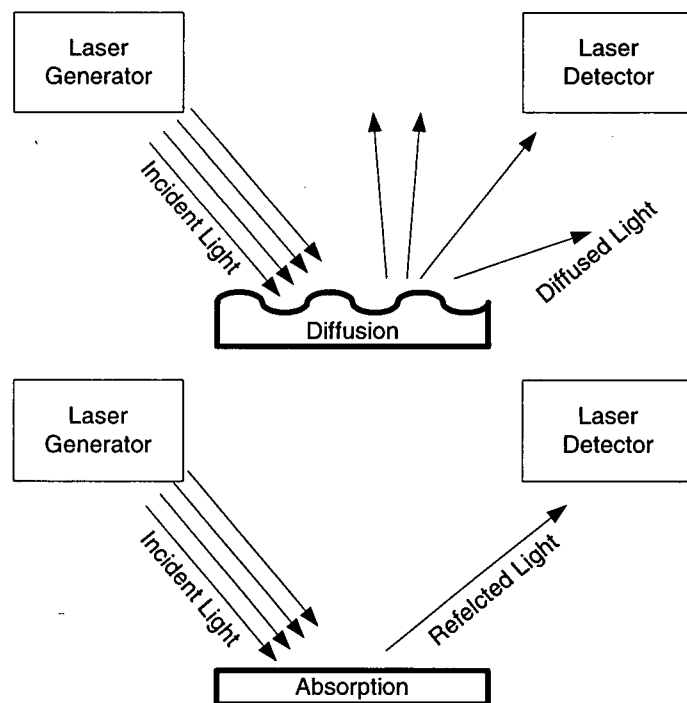
Figure 20 Illustrations of Diffusion and Absorption

Four carrier modifications based on either the diffusion or absorption methods are tested:

1. Silk-screening. By applying heat thru a fine silk screen, the carrier surface is slightly melted to create a coarse surface that diffuses the incident focus laser beam.

2. Sanding. By sanding the surface of the carrier with fine sand paper, a coarse surface is created. Sand papered surface appears rougher than the silkscreen surface thus shall have better diffusing characteristics

3. Paint with coarse finish. By painting the carrier with flat black paint with a coarse finish, this surface shall both diffuse and absorb the incident focus laser beam.

4. Paint with smooth finish. By painting the carrier with flat black paint with a smooth finish, this surface shall absorb the incident focus laser beam.

As shown in Figure 21, the two painting methods that absorb the focus laser reduce the signal strength more effectively than the others.
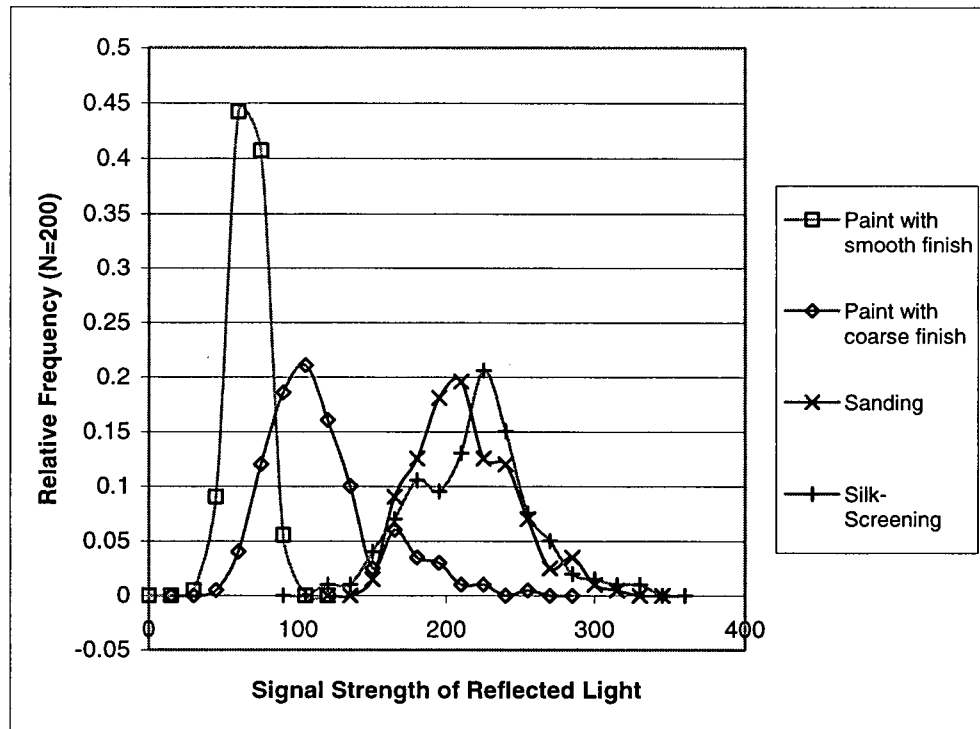
Figure 21 Reflective Properties of Various Surfaces

Further more, the paint with smooth finish method, in addition to being the least reflective surface among the four, also deviates from its mean the least due to its smooth surface. The signal profile for smooth painted surface has a standard deviation of 10.9, while all other surfaces that diffuse light deviate significantly from their means with standard deviations ranging from 32 to 38. In summary, the paint with smooth finish method yields the best result in improving the on-carrier signal profile and is used for all following works presented in this thesis.

One other factor to consider for improving the on-carrier signal profile is the performance of the algorithm under harsh sensing conditions such as degradation of the focus laser generator's output over time. The power level outputted by the

focus laser generator decreases as its laser diode ages. Therefore, to ensure the long-term reliability of the edge detection algorithm, on-paper and on-carrier signal profiles with decreased focus laser power level need to be investigated. To simulate the reduced performance of laser diode, the laser output is reduced from 100% to 75% then 50% and the on-carrier signal profiles, as well as the on-paper signal profiles, are sampled and graphed as shown in Figure 22 and Figure 23.
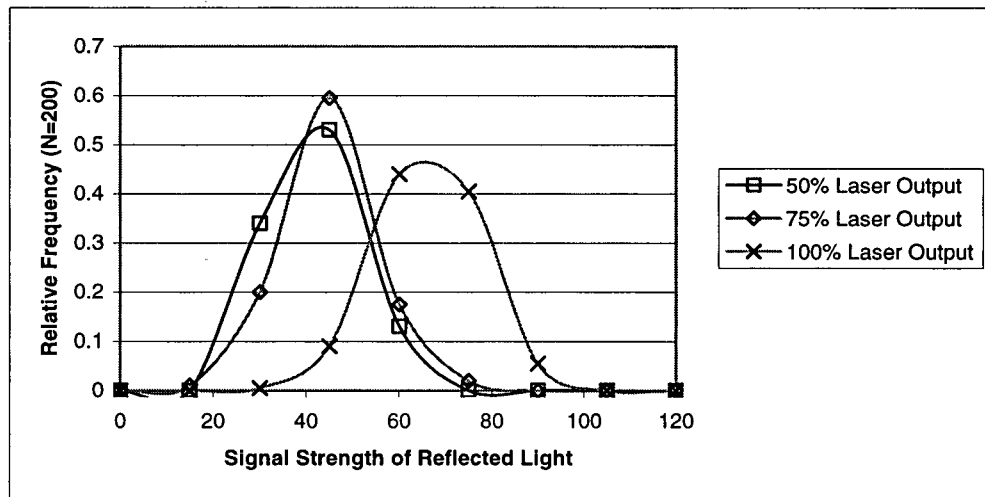
Figure 22 On-Carrier Signal Strength at Various Laser Output
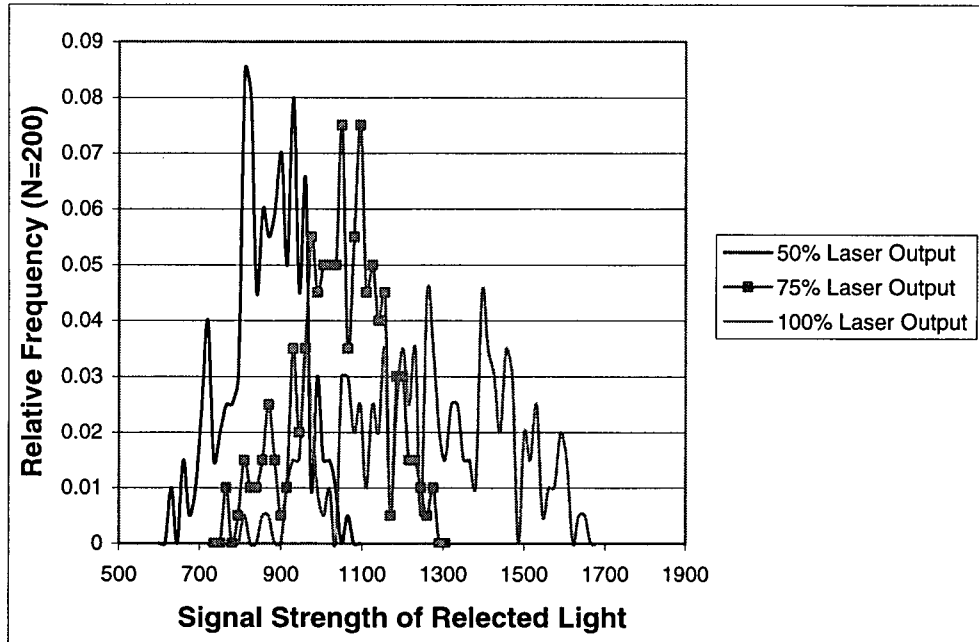
Figure 23 On-Paper Signal Strength at Various Power Output

As expected, when laser output is reduced, the levels of reflected light are also reduced. However, the strength of on-paper signal does not drop significantly. The strength of on-carrier is also reduced following the drop in laser output. Even with 50% of laser output, the reflected light level differences between the paper and painted carrier are still large enough for a reliable threshold to be established.

4.5   Threshold Selection

The requirement for a reliable threshold is that any sample below the threshold must has at least 99.5% probability of being the result of focus laser reflected by the carrier. According to Chebyshev's theorem, if the threshold is selected at k times the standard deviation from the mean of the on-carrier signal, the probability of any sample above the threshold is the result of focus laser reflected

54

by the proof sheet is at least $1 - \dfrac{1}{k^2}$. Thus, to achieve 99.5% probability, k must be at least 14 [8]. Therefore, the threshold t can be calculated by:

$$t = \mu + k\sigma$$

where μ is the mean and σ is the standard deviation of the signal. Table 1 shows the parameters required for selecting the threshold at different power levels.

Power Level	On-carrier Signal Mean (μ)	On-carrier Signal Standard Deviation (σ)	Calculated Threshold (t)
100%	59.0	9.5	167
75%	38.0	9.8	175
50%	34.9	10.9	*212*

Table 1 Parameters Used for Threshold Calculation

To ensure the threshold remains reliable even when the laser diodes' performance degrades, the calculated threshold at 50% power level is chosen.

4.6 Edge Signal Profiles

In addition to a threshold that distinguishes between on-paper and on-carrier reliably, the edge detection algorithm requires a sharp signal transition between the two states in order to measure the edge position accurately. Therefore, the signal profiles near the edges of the proof sheet needs to be studied in detail. To obtain the main-scan edge signal profiles near M_1 as shown in Figure 24, the

focus laser is moved from M_{S1} to M_{S2} by sub-scan actuation at a constant velocity and while sampling the reflected light level every 50μm.
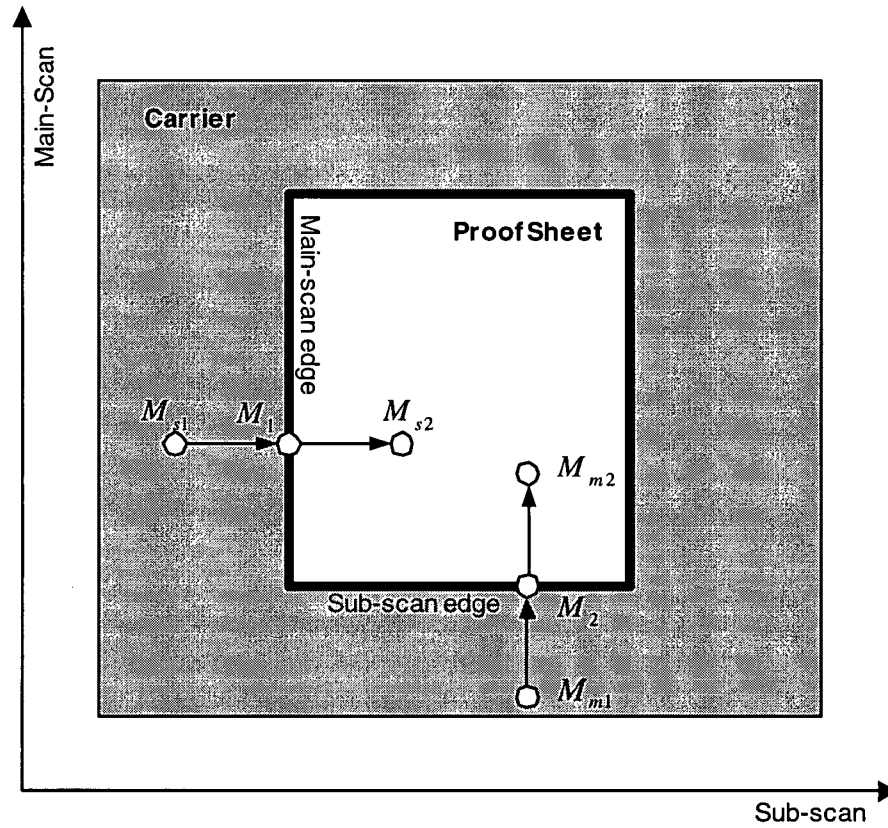
Figure 24 Paths of Focus Laser for Obtaining Edge Signal Profiles

The result is shown in Figure 25.
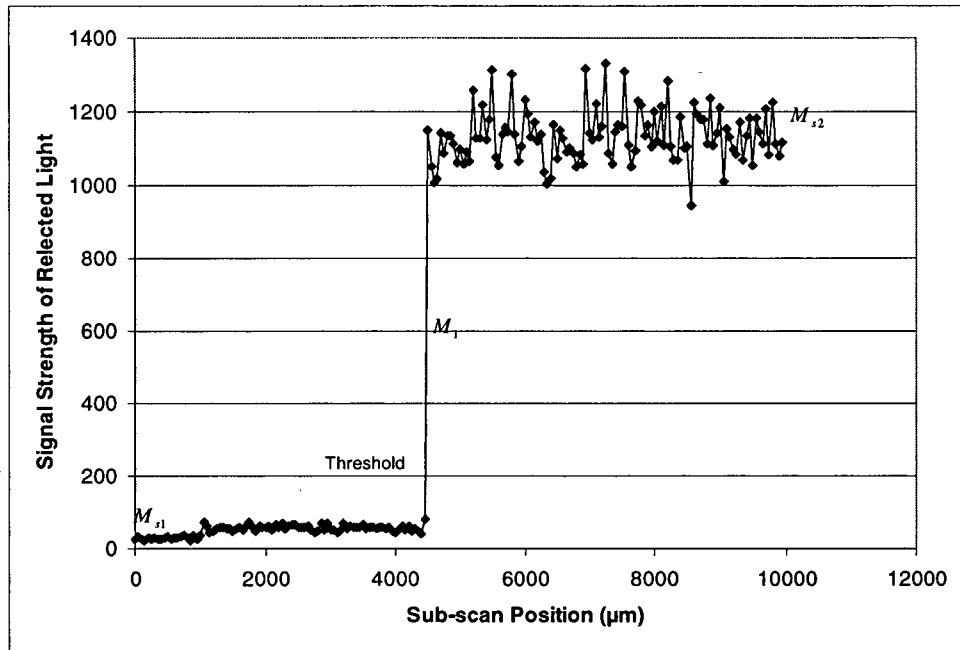
Figure 25 Main-scan Edge Signal Profile

As shown in Figure 25, the transition from below to above the threshold at the main-scan edge is very sharp and the threshold clearly differentiates between the two states.

To obtain the sub-scan edge signal profiles near M_2 as shown in Figure 24, the focus laser is moved from M_{m1} to M_{m2} by main-scan actuation at a constant velocity while sampling the reflected light level every 50 μm. The result is shown in Figure 26.
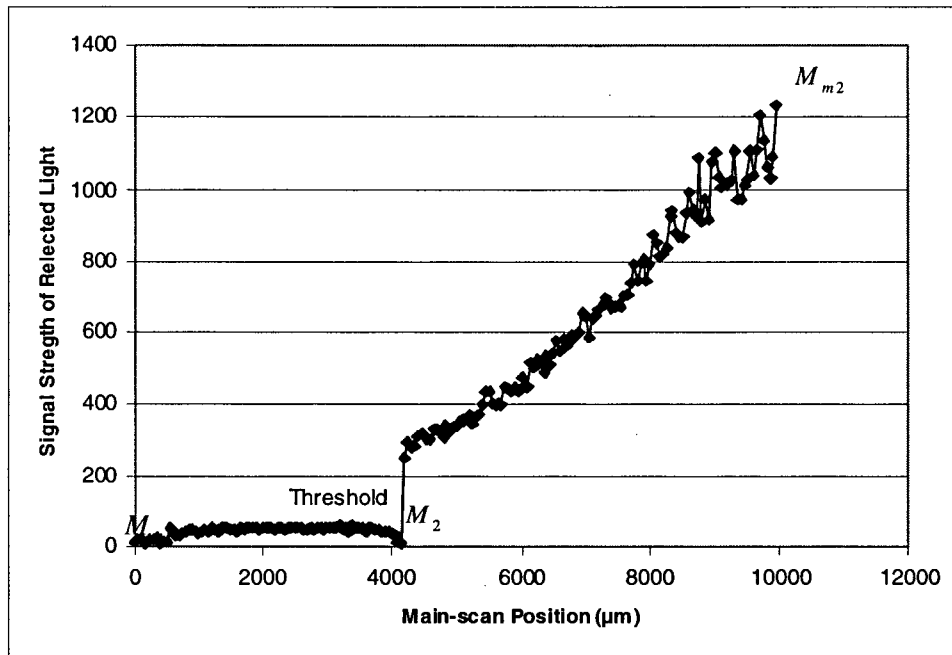
Figure 26 Sub-scan Edge Signal Profile

Even through the signal crosses from below to above the threshold sharply at the main-scan edge, the on-paper region of the signal appears to be not as well defined as the main-scan edge profile. This is caused by small gaps between the proof sheet and the carrier near the sub-scan edges. The proof sheet is held by two rows of vacuum holes on the carrier near the sub-scan edges as shown in Figure 27.
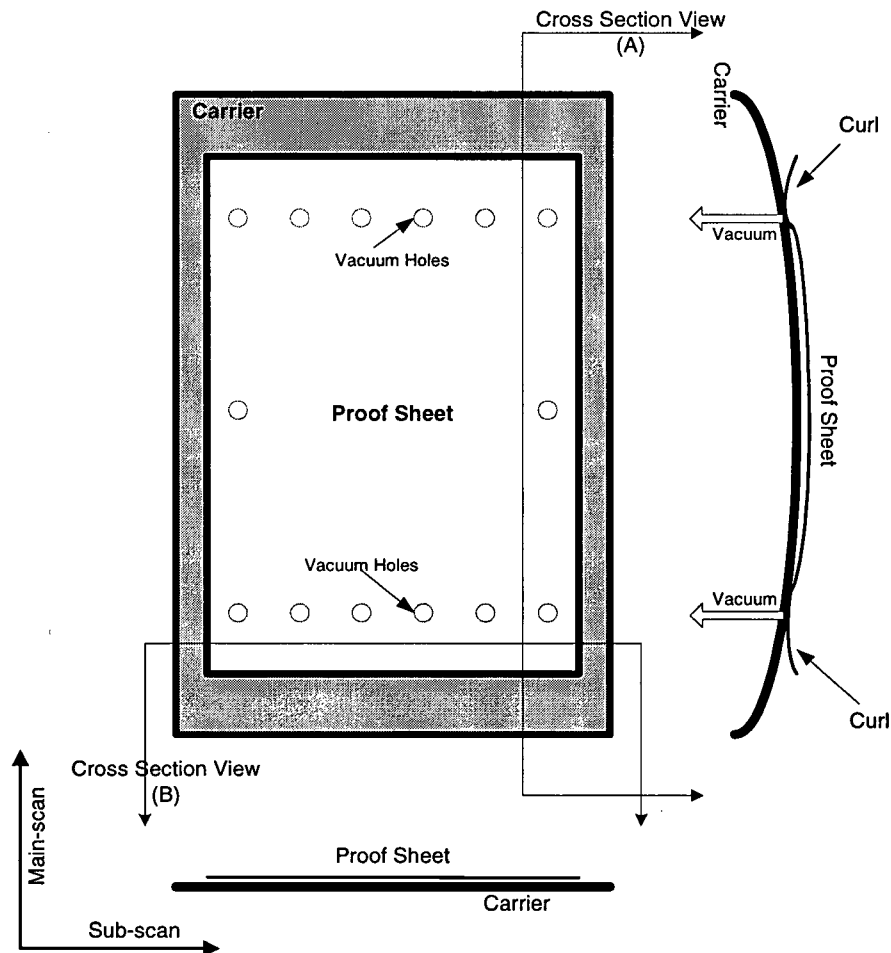
Figure 27 Proof Sheet on Carrier

Because of the arrangement of the vacuum holes, the sub-scan edges curl away slightly from the carrier (as shown in the cross section view (A) in Figure 27) resulting in curved surfaces that reflect the focus laser less effectively comparing to flat surfaces. On the other hand, the main-scan edges do not exhibit the same physical characteristics (as shown in the cross section view (B) in Figure 27) since the proof sheet is rolled on the carrier from the top row of the vacuum holes to

59

the bottom row of the vacuum holes. The rolling action seals and tucks the proof sheet, thus ensuring solid contact between the proof sheet and the carrier along the main-scan edge.

The edge curl causes the detection of edge position to be inconsistent. When donor is loaded on top of the proof sheet, it forces the curled edges down, thus the edge position changes as shown in Figure 28.
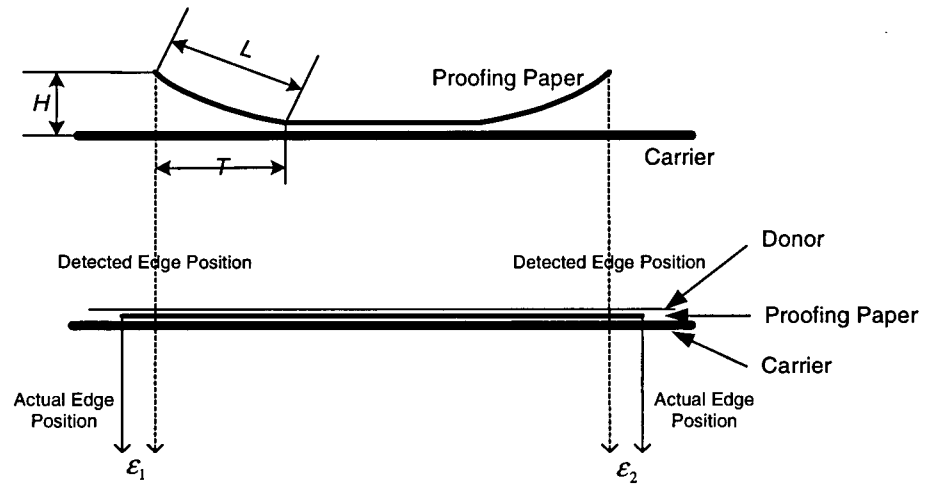
Figure 28 Errors Caused by Edge Curls

Since the gap between the edge and the carrier is relatively small, the error caused by edge curls, namely ε_1 and ε_2, can be estimated by:

$$\varepsilon_x = L_x - T_x = L_x - \sqrt{L_x^2 - H_x^2}$$

where $L_x = 21 \pm 5$ (mm) and $H_x \cong 2$ (mm). Therefore, the estimated error is $\varepsilon_x \cong 95 \pm 24$ (µm). Since the variation in ε_x is negligible, a constant curl effect

error $\varepsilon = 95$ (µm) is used by geometric correction to compensate the edge curl effect.

4.7   Implementation of Main-scan Edge Detection Algorithm

The main-scan edge detection algorithm involves of the software and hardware control modules as shown in Figure 29, where the shaded blocks are functions implemented specifically for the purpose of adding the backup registration feature.

Figure 29 Implementation of Main-scan Edge Detection Algorithm

To start edge detection, the main-scan edge detection control signals the edge detection function that turns on the focus laser and switches the A/D converter

to continuous mode. While in continuous mode, the A/D will sample the analog light level and convert to digital values every 20 ms. When one conversion is completed, an interrupt is generated to the head controller then the next conversion is started. The threshold comparison ISR compares the converted light level with the pre-defined threshold. If threshold-crossing event occurs, then the ISR toggles the threshold-crossed line to high, stops the A/D converter, and turn off the focus laser.

On the main controller, the main-scan edge detection control commands the sub-scan actuation to start moving toward the edge of the proof sheet and signals the head controller's edge detection function to start its sequences. Then, the threshold-crossing interrupt is enabled to monitor for the rising edge of the threshold-crossing line. As soon as the threshold-crossing line is pulled high by the head controller, the threshold-crossing ISR is run which latches the current sub-scan position as the edge position and stop the sub-scan actuation. The latched position is the measured main-scan edge position.

4.8   Implementation of Sub-scan Edge Detection Algorithm

The main-scan edge detection algorithm involves of the software and hardware control modules as shown in Figure 30 where the shaded blocks are functions implemented specifically for the purpose of adding the backup registration feature.
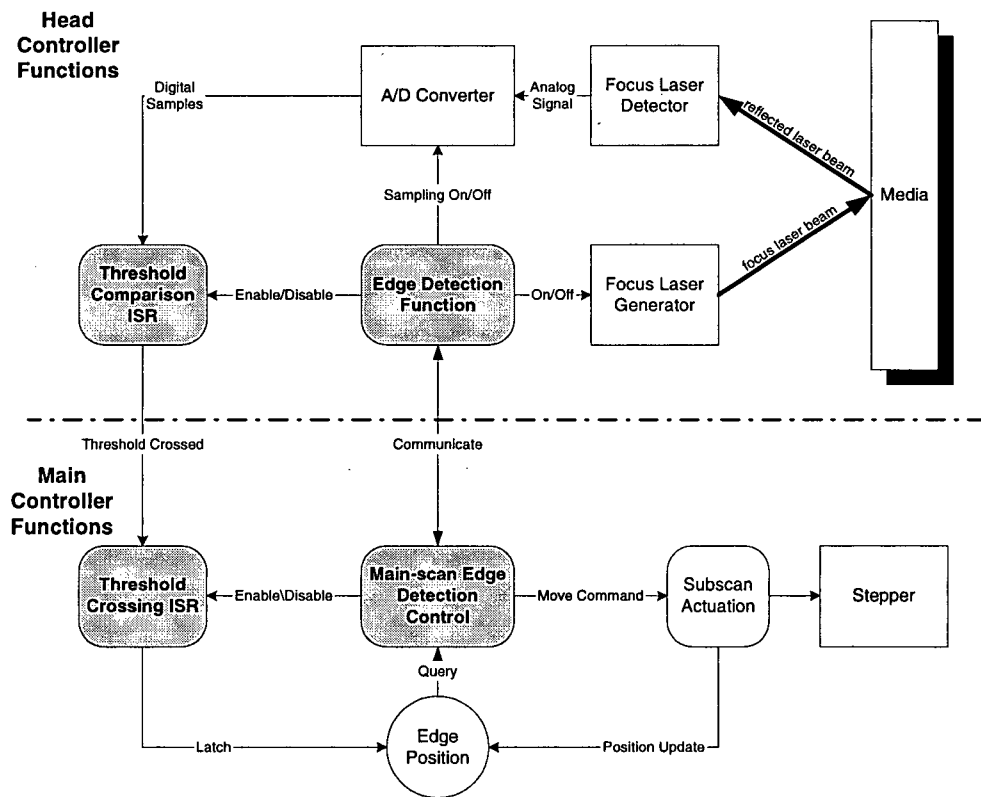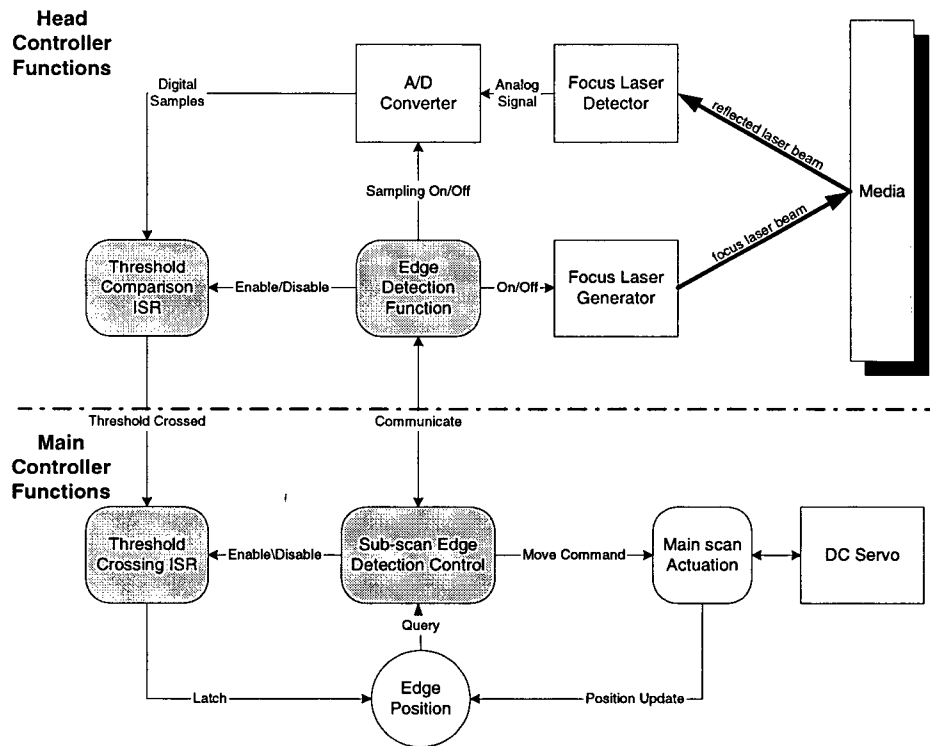
Figure 30 Implementation of Sub-scan Edge Detection Algorithm

The differences in this algorithm compared to the main-scan edge detection are:

1. The focus laser is moved by the main-scan actuation instead of sub-scan actuation.

2. There are two direction of focus laser travel in sub-scan edge detection. To detect the front side points M_3 and M_4, the focus laser needs to travel from the bottom up. To detect the backside points M_3' and M_4', the focus laser needs to travel from the top down.

Therefore, the edge detection function, the threshold comparison ISR, and the threshold crossing ISR are routines shared between the main and sub-scan edge detection processes. The design specifications for these functions are discussed in Appendix B.

4.9   Test Results

The effectiveness of the geometric detection process is measured by the repeatability of the results. That is, for the geometric process to be effective, the results collected at the same position must have small variation among them. By repeating the detection process at the same main-scan and sub-scan edge points, a large number of samples are collected. The distributions of the relative frequency of the samples are studied to estimate the accuracy of the geometric detection process.

The distribution of the main-scan edge detection samples is shown in Figure 31.
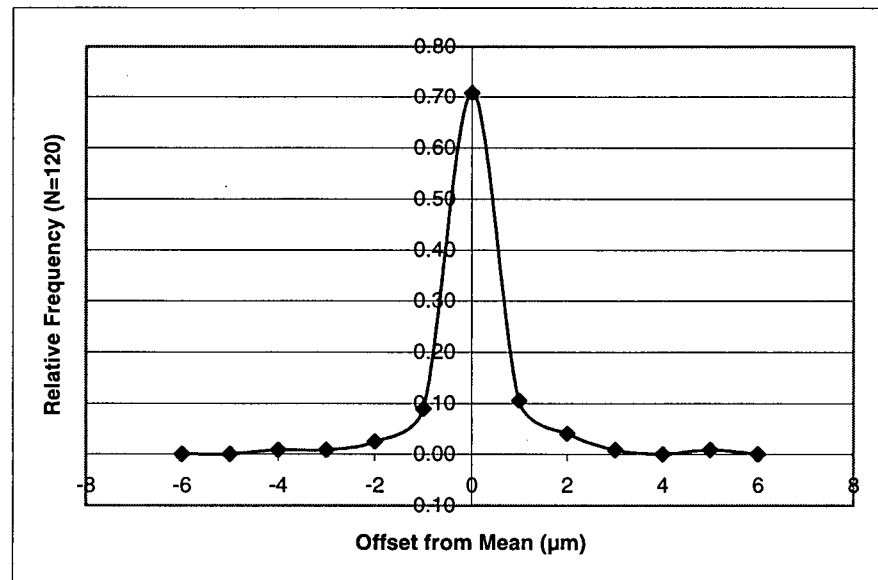
Figure 31 Distribution of Main-scan Edge Detection Samples

As shown in the figure above, all of the main-scan edge detection samples fall within ±5μm of the mean. The accurate result is due to the precision of the sub-scan actuation hardware that is capable of providing the current position of the focus laser with 1μm of precision. With the slow traveling speed of the focus laser and the high sampling rate, the threshold is being compared at least once per μm. With the small variation of the main-scan edge detection, the rotation of the proof sheet derived from these results will also be consistent from measurement to measurement.

In contrast to the previous results, the distribution of the sub-scan edge detection samples varies significantly as shown in Figure 32.
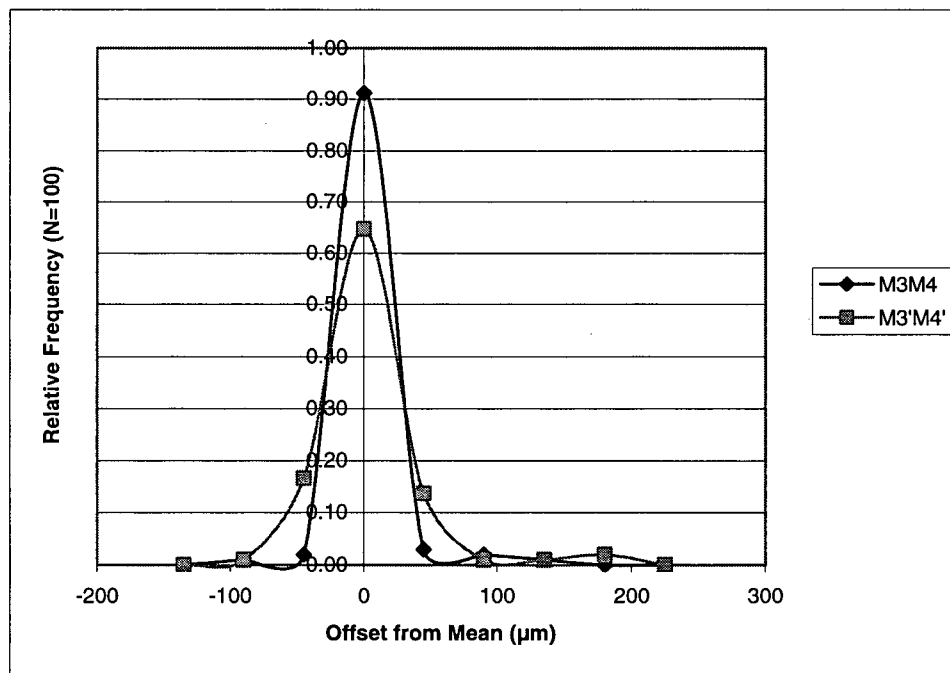
Figure 32 Distributions of Sub-scan Edge Detection Samples

The figure shows the distribution of the front side detection in the M3M4 series as well as the backside detection in the M3'M4' series. The two series exhibit similar characteristics thus the difference between detecting the sub-scan edges from the top down versus from the bottom up is negligible. As shown, all of the sub-scan edge detection samples fall within ±250μm of the mean. The result is due to the precision of main-scan actuation during moving the focus laser which is 45μm. Comparing to the 1μm precision of the sub-scan actuation, one can expect the overall accuracy of the sub-scan edge detection is roughly 45 times of the main-scan edge detection, or ±225μm. The result agrees with the expectation. Interestingly, the difference between the main-scan and sub-scan signal profiles near the edges does not contribute significantly to the variation of the results possibly due to the ability of the chosen threshold to distinguish between on-paper and on-carrier signals.

From the results above, one can expect that the two-sided proofs show minimal misalignment between the front and the back images in the sub-scan direction with observable misalignment in the main-scan direction. In order to estimate the amount of main-scan misalignment of the backup registration, the joint probability of the front side detection series (M3M4) and the backside detection series (M3'M4') is studied.

Assuming x represents the offsets from mean for M3'M4' while y represents the offsets from mean for M3M4, their joint probability function can be defined as

$$f(x, y) = P(X=x, Y=y);$$

that is, the values $f(x, y)$ give the probability that outcomes x and y occur at the same time. Table 2 shows the values of $f(x, y)$.

66

f(x,y)		x (μm)							Row Totals
		-90	-45	0	45	90	135	180	
y (μm)	-90	0.01%	0.16%	0.63%	0.13%	0.01%	0.01%	0.02%	0.98%
	-45	0.02%	0.33%	1.27%	0.27%	0.02%	0.02%	0.04%	1.96%
	0	0.89%	15.20%	59.00%	12.51%	0.89%	0.89%	1.79%	91.18%
	45	0.03%	0.49%	1.90%	0.40%	0.03%	0.03%	0.06%	2.94%
	90	0.02%	0.33%	1.27%	0.27%	0.02%	0.02%	0.04%	1.96%
	135	0.01%	0.16%	0.63%	0.13%	0.01%	0.01%	0.02%	0.98%
	180	0.00%	0.00%	0.00%	0.00%	0.00%	0.00%	0.00%	0.00%
Column Totals		0.98%	16.67%	64.71%	13.73%	0.98%	0.98%	1.96%	100.00%

Table 2 Joint Probability Distribution of Sub-scan Edge Detections

Since the amount of main-scan misalignment in the final proof images is *y-x*, its distribution can be calculated from the table above. Figure 33 shows the distribution of estimated main-scan misalignment.
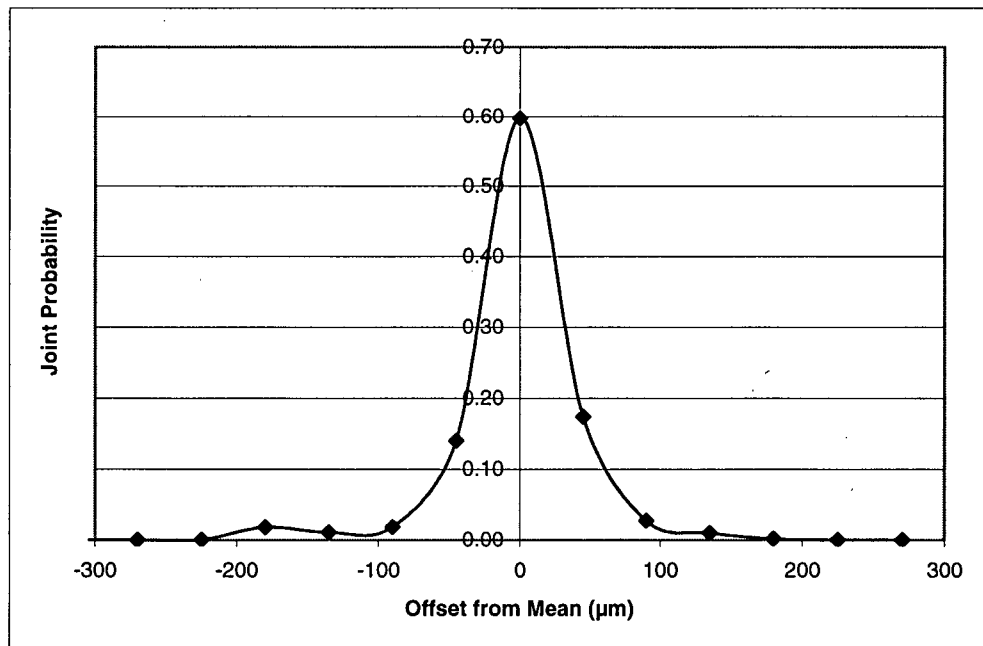
Figure 33 Distribution of Misalignments between Front and Back Images

In summary, the errors in backup registration of the two-sided proof due to variation in geometric detection are to be within 300μm in the main-scan and within 5μm in the sub-scan. These results are within the 1mm backup registration requirement, thus, the proposed geometric detection methods shall be capable of providing the parameters needed by geometric correction.

Chapter 5

GEOMETRIC CORRECTION

The geometric correction process shifts and rotates both the front and the back images such that they registered on the two-sided proof. The process consists of three operations: shift correction, rotation correction, and raster data mirroring. The process depends on the edge positions detected during geometric detection.

The shift correction moves the origin of the image to the position determined by the detected edge positions. In addition, shift correction also compensates for factors such as image margins, edge curl effects, and write-laser offsets. To ensure that all separations of an image are registered, the same shifts must be applied to during imaging each separation. The Spectrum proofers support image shifts to any position on the proof sheet thus the only implementation requirement for supporting backup registration is to derive the appropriate amount of shifts in the main and sub-scan directions.

The rotation correction rotates the image with respect to its origin by the specified angle. It consists of two operations: sub-scan shearing and main-scan shearing. To implement sub-scan shearing on Spectrum, its existing orthogonal correction algorithm, a form of raster correction, needs to be modified such that it supports various shearing angles. For main-scan shearing, a novel approach of manipulating the starting point of each swath is implemented. To avoid observable image artifacts due to main-scan shearing, the difference of starting point from swath to swath is limited to one image pixel. Therefore, the rotation correction is only capable of correcting small angle rotation.

To ensure the back image registers with the front, it must be plotted as mirrored since the proof sheet is flipped. In the proposed process, the sheet is flipped with respect to the sub-scan axis or vertically. Therefore, the raster data for the back image must also be flipped in the same manner. By reversing the direction of raster data entering the buffer in the data path, this function can be added to the existing Spectrum proofer.

5.1   Shift Correction

To shift a image on the Spectrum proofer, the amount of shifts from the origin of the imaging system to the origin of the image data must be specified in terms of main and sub-scan components. As discussed in section 3.2, for backup registration, the origin of the image data for the front image is:

$$I_0 = A + R_\theta \vec{w}.$$

The origin for the back image is:

$$I_1' = A' + R_\delta R_f (\vec{w} + L \cdot \vec{j}).$$

Since R_f and L are known constants, A, A', R_θ, and R_δ can be calculated from the edge detection points obtained during geometric detection. The only variable that needs to be looked at is $\vec{w}$. The main and sub-scan components of $\vec{w}$ can be expressed as:

$$\vec{w} = w_s \vec{i} + w_m \vec{j} \qquad\qquad \text{Equation 23}$$

where w_s is the sub-scan component in μm while w_m is the main-scan component in μm. The sub-scan component w_s consists of three variables, sub-

70

scan image margin m_s, write laser sub-scan offset l_s, and blank padding shift ρ_s as represented in Equation 24.

$$w_s = m_s + l_s + \rho_s$$
<div align="right">Equation 24</div>

The blank padding ρ_s is discussed in section 5.2.1

The main-scan component w_m also consists of three variables, main-scan image margin m_m, write laser sub-scan offset l_m, and curl effect constant ε as represented in Equation 25.

$$w_m = m_m + l_m - \varepsilon$$
<div align="right">Equation 25</div>

The curl effect constant ε has been discussed in detail in section 4.6.

5.1.1 Image Margin

Most of press sheets have non-print margins around the printed images to accommodate the paper being removed during trimming. Therefore, it is important for proofs to show the same margins as the press sheets. The width of the margin is specified through the user interface and passed down to the data path on the Spectrum proofer. The test proofs produced for studying the proposed process has a ½" margin all around the image thus $m_s = m_m = 12.7 (mm)$.

5.1.2 Write Laser Offsets

The Spectrum proofer images the raster data with its thermal write laser. However, edge detection positions are detected using the focus laser in geometric detection. Thus, the physical offsets between the write laser beam and the focus

laser beam on media must be measured and compensated. Figure 34 represents the offsets graphically.
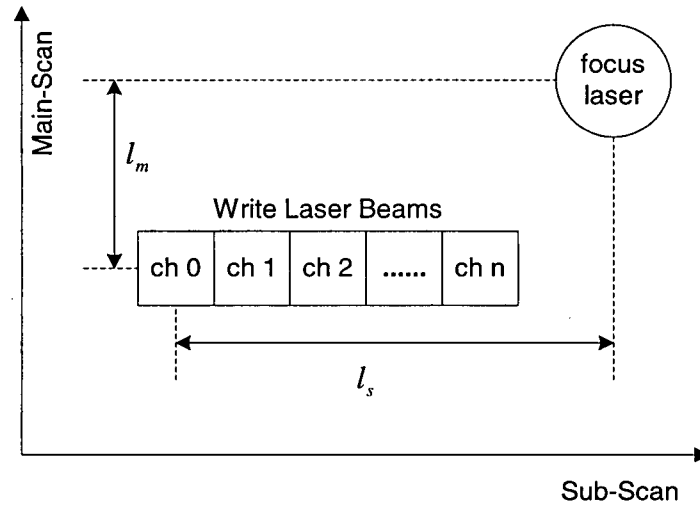
Figure 34 Illustration of Write and Focus Laser Offsets

The offsets are measured on the Spectrum used for producing test proofs as the following:

$$l_s = 2570(\mu m)$$

and

$$l_m = 460(\mu m) .$$

5.2 Rotation Correction

To rotate an image with respect to its origin, a method of combining main-scan shearing and sub-scan shearing is proposed to make use of existing Spectrum

72

functionality and hardware. The main-scan and sub-scan shearing are shown in Figure 35.

Figure 35 Main-scan and Sub-scan Shearing

From geometric detection, the rotation angles of the proofing sheet, θ for the front and δ for the back, are obtained. Thus, the required angles of rotation

correction are $\theta_R = \theta$ for the front and $\theta_R = \delta$ for the back. The amount of main and sub-scan shearing is given by $\theta_m = \theta_s = \theta_R$.

The sub-scan shearing utilizes the exiting orthogonal correction algorithm on the Spectrum and is discussed in section 5.2.1. A new algorithm for main-scan shear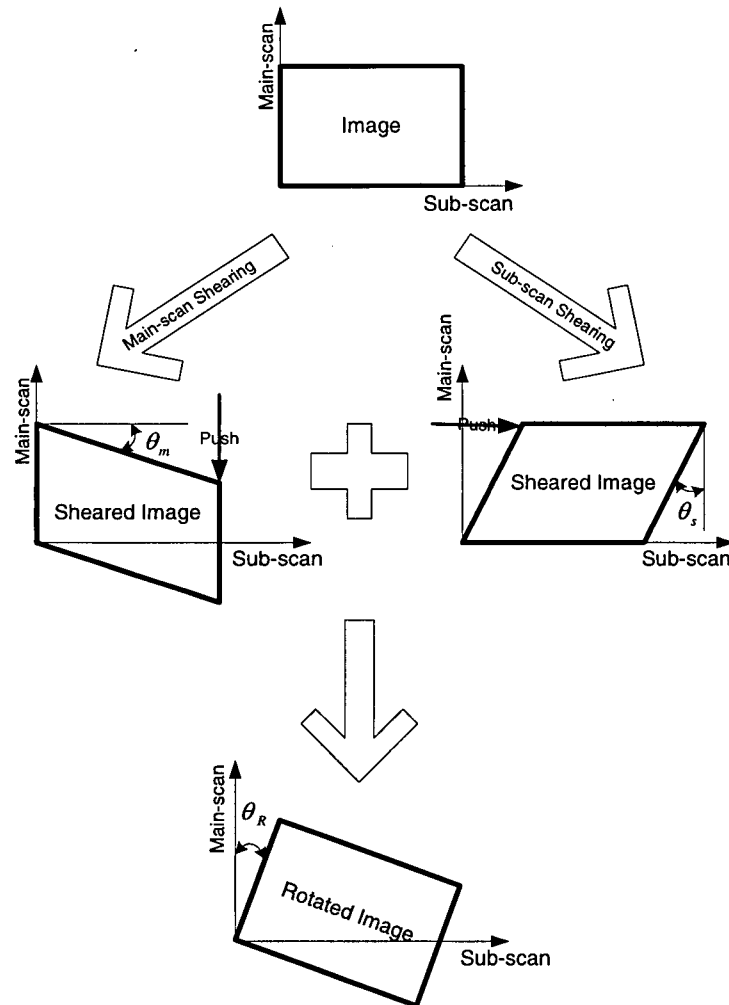ing that controls the starting positions of each image swath is discussed in section 5.2.2. In section 5.2.3, the side effects of geometric rotation, namely the image artifacts and scaling errors are examined.

5.2.1 Sub-scan Shearing

Due to the orientation of the drum and the continuous motion of the laser head during imaging (see Figure 12 in Chapter 2), when swaths of the raster data are imaged on the media, the swath direction is not parallel to the main-scan direction nor perpendicular to the sub-scan direction. The angle between the main-scan direction and the swath direction, $\angle \sigma$, is known as the orthogonal angle. The circumference of the drum ϕ (µm) and the swath width ω (µm) determines σ and is expressed in Equation 26.

$$\sigma = \tan^{-1} \frac{\omega}{\phi}$$

Equation 26

The orthogonal angle causes the rectangular image data to appear on the media as a parallelogram. This effect, as shown in Figure 36, is known as helical distortion.

74
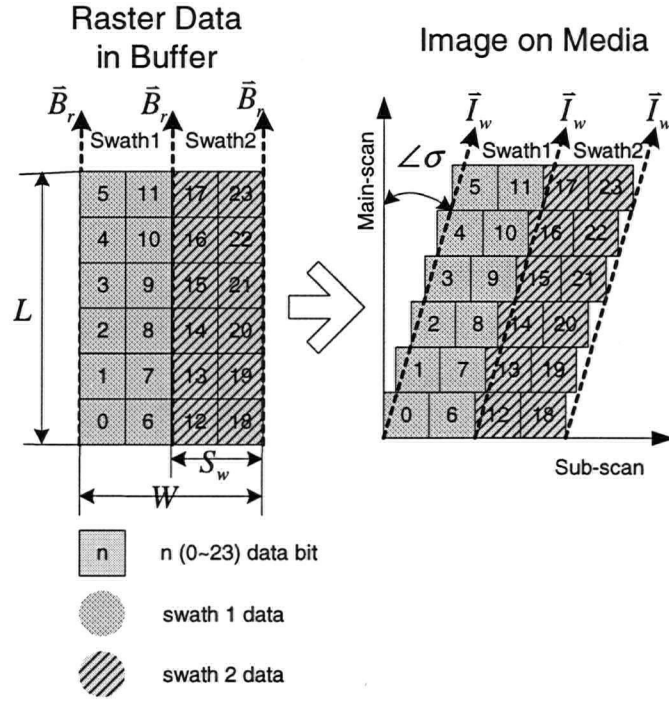
Figure 36 Illustration of Helical Distortion

In the example above, a raster data of 6 pixels by 4 pixels is to be imaged on the media in swathes of 2 pixels wide. Thus, the image length L is 6 pixels; the image width W is 4 pixels; and the pixel per swath S_w is 2 pixels. In addition to Equation 26, the orthogonal angle $\angle\sigma$ can be calculated by:

$$\sigma = \tan^{-1}\frac{S_w}{L} \qquad\qquad \text{Equation 27}$$

Figure 36 also shows the direction of the raster data being read from the buffer $(\vec{B}_r)$ and the direction of the data being imaged on to the media $(\vec{I}_w)$.

To compensate for helical distortion, the data path on Spectrum outputs swaths of raster data at an angle such that the resulting image on the media appears rectangular. This method of compensation is called orthogonal correction and is shown in Figure 37.

Figure 37 Illustration of Orthogonal Correction

The orthogonal correction process can be divided into the following steps:

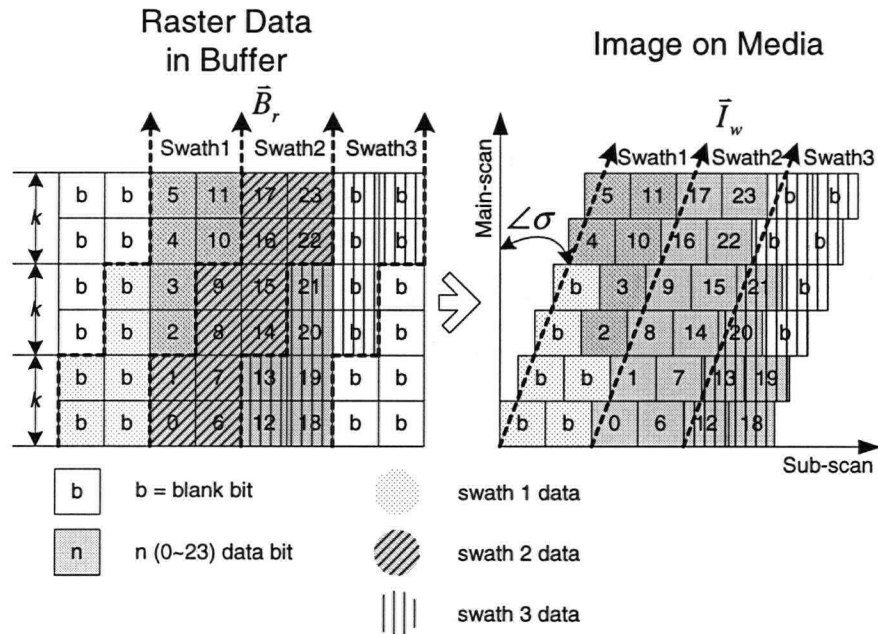1. Prior to buffering the first swath of raster data, fill one swath of zero (the blank bits) at the start of the buffer as blank padding. The width of blank padding is ρ bits and for orthogonal correction, $\rho = S_w$.

2. Fill the buffer with swaths of raster data bits.

76

3. When imaging, read the raster data in the buffer from the bottom up and shift the pointer in the sub-scan by one bit after every k main-scan bits are read. The factor k is known as the correctional frequency and is calculated by $k = \dfrac{L}{\rho}$. The result of this is the swaths are read from the buffer at an angle.

4. Pad one extra swath of blank bit at the end of the raster data such that the last swath imaged on the media only contains valid raster data.

This method of compensating for helical distortion is also called raster correction because the raster data is manipulated. Although the misalignments among most pixels on plotted images are negligible such as between pixel 0 and pixel 1, shifts of roughly one pixel appears every k pixels such as between pixel 3 and pixel 4. These one pixel wide shifts are know as raster correction artifacts. The pixel size of the Spectrum is 10μm by 10μm thus the raster correction artifacts are unobservable and the images appear orthogonal by the naked eyes.

To shear the image by θ_s as shown in Figure 35, the orthogonal correction algorithm needs to be modified such that ρ can vary depending on θ_s and the shifting of pointer while reading the buffered data can be done in either the positive or the negative sub-scan direction. To determine the relationship between ρ and θ_s, the following four cases of θ_s are investigated:

1. $\theta_s = 0$.

2. $\sigma \geq \theta_s > 0$.

3. $\theta_s < 0$.

4. $\theta_s > \sigma$.

Figure 38 represents case 1, $\theta_s = 0$, graphically.
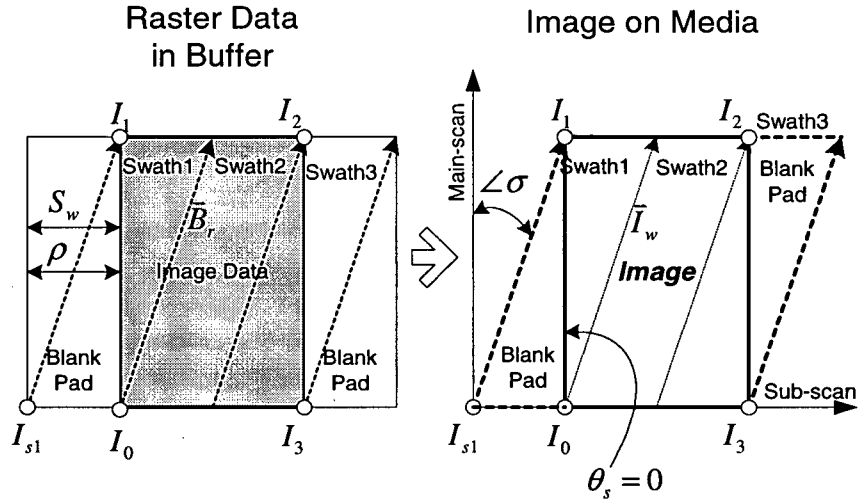
Figure 38 Illustration of Sub-scan Shearing, Case 1

Note the positions of selected data points:

I_{s1}: starting point of Swath 1,

I_0: image origin, same as the starting point of Swath 2 I_{s2} in this scenario,

I_1, I_2, and I_3: corner points of the image,

and their corresponding positions on the media are identical. In addition, the slope of $\vec{B}_r$ is the same as the slope of $\vec{I}_w$. In the case of $\theta_s = 0$, there is no sub-

scan shearing as of orthogonal correction thus the amount of blank pad is $\rho = S_w$. The blank padding shift ρ_s can be calculated by:

$$\rho_s = \rho \times \frac{\omega}{S_w}$$

where $\dfrac{\omega}{S_w}$ is the width of an image pixel on the media in μm.

For case 2, $\sigma \geq \theta_s > 0$, the amount of blank padding ρ needs to be decreased, as shown in Figure 39.

Figure 39 Illustration of Sub-scan Shearing, Case 2
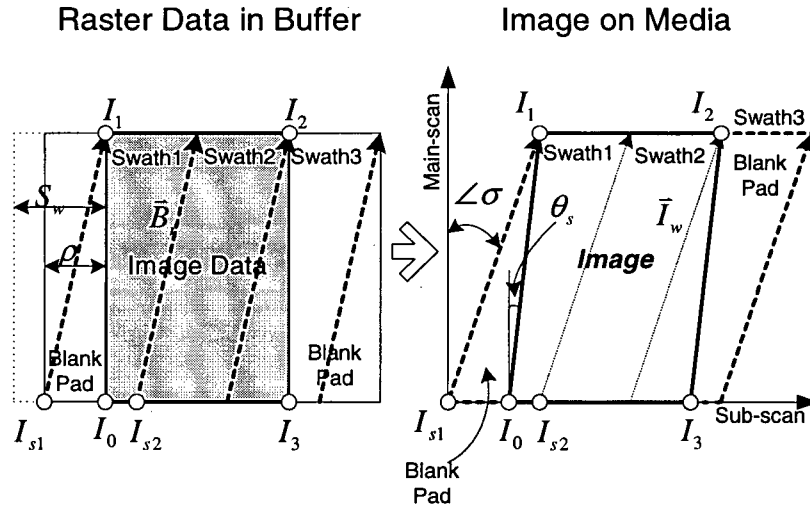
Since $\rho < S_w$, the slope of $\bar{B}_r$ is greater than that of $\bar{I}_w$. For the blank padding shift ρ_s, Equation 28 still holds for this scenario. To derive ρ from θ_s, the Swath 1 region of the Image on Media is expanded and shown in Figure 40.
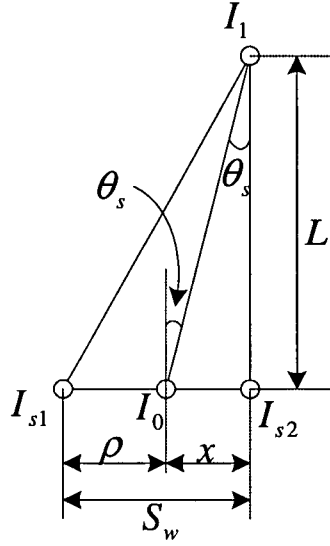
Figure 40 Expanded View of Sub-scan Shearing, Case 2

From the illustration above, $\tan \theta_s = \dfrac{x}{L}$ where $x = S_w - \rho$. Therefore,

$\tan \theta_s = \dfrac{S_w - \rho}{L}$ so $\rho = S_w - L \tan \theta_s$. Since the sine and cosine of the rotation

angle is obtained from the geometric detection process, it is desirable to express

ρ as in Equation 29.

$$\rho = S_w - L\left(\frac{\sin \theta_s}{\cos \theta_s}\right)$$

Equation 29

When $\theta_s = \sigma$, $\tan \theta_s = \dfrac{S_w}{L}$, thus $\rho = 0$. The image produced for this special

case is the same as images produced without orthogonal correction.

For case 3, $\theta_s < 0$, the slope of $\bar{B}_r$ needs to be smaller than that of $\bar{I}_w$, thus $\rho > S_w$, as shown in Figure 41.

Raster Data in Buffer   **Image on Media**
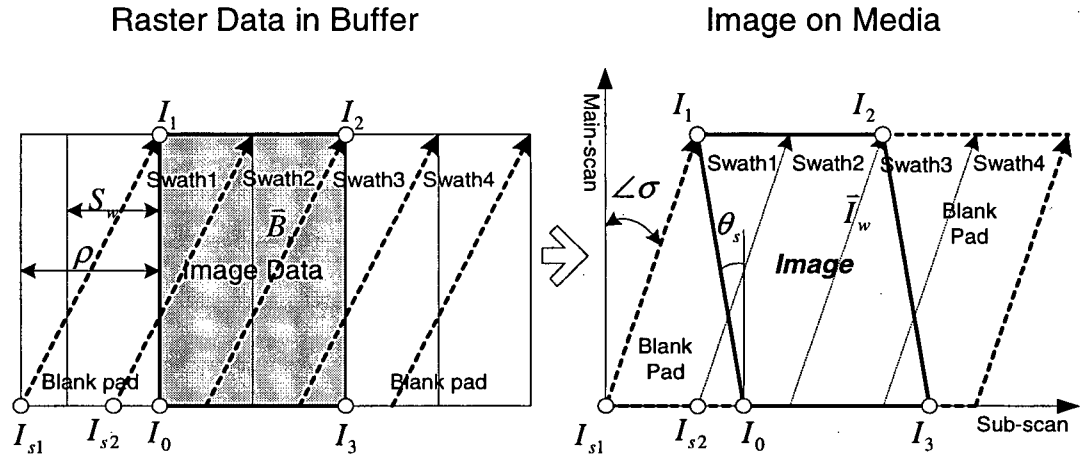
Figure 41 Illustration of Sub-scan Shearing, Case 3

The blank padding shift ρ_s in this case can also be calculated from Equation 30. Similarly, the region near Swath 1 of Image on Media is expanded in Figure 42 for deriving ρ from θ_s.
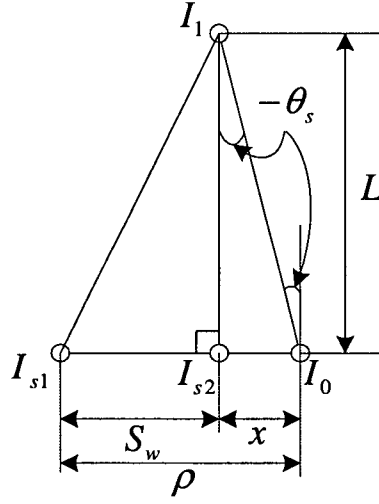
Figure 42 Expanded View of Sub-scan Shearing, Case 3

Because $\theta_s < 0$, the angle $\angle I_{s2}I_1I_0 = -\theta_s$ while $\tan(-\theta_s) = \dfrac{\rho - S_w}{L}$. Since

$\tan(-\theta_s) = -\tan\theta_s$, $-\tan\theta_s = \dfrac{\rho - S_w}{L} \Rightarrow \rho = S_w - L\tan\theta_s$ can be derived. The

result is identical to Equation 29.

Case 4, $\theta_s > \sigma$, represents the most challenges in terms of implementation. As

shown in Figure 43, the direction of $\vec{B}_r$ is in reverse compares to that of $\vec{I}_w$.

RasterData
inBuffer

ImageonMedia

Figure 43 Illustration of Sub-scan Shearing, Case 4

Since the image origin I_0 is the first pixel being imaged in this scenario, there is no need for blank padding shift thus $\rho_s = 0$. Again, the region near swath 1 is expanded and shown in Figure 44.

Figure 44 Expanded View of Sub-scan Shearing, Case 4

Here, $\tan\theta_s = \dfrac{S_w + \rho}{L}$ and ρ is expressed in the sine and cosine of θ_s in Equation 31.

$$\rho = L\left(\frac{\sin\theta_s}{\cos\theta_s}\right) - S_w \qquad\qquad \text{Equation 31}$$

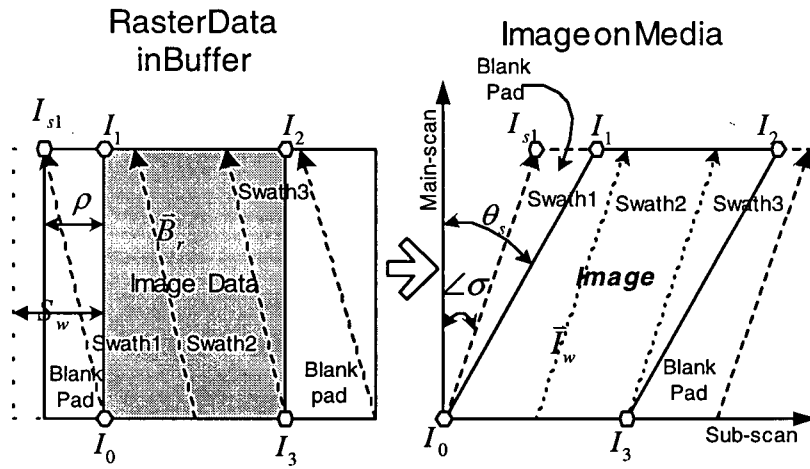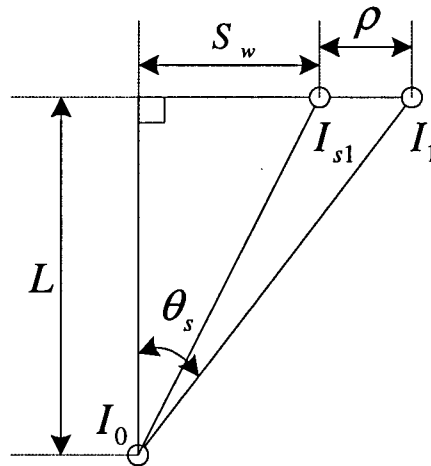In summary, when the angle of shearing is less than the orthogonal angle $(\theta_s \leq \sigma)$, the amount of blank padding ρ can be derived from $\rho = S_w - L\left(\dfrac{\sin\theta_s}{\cos\theta_s}\right)$ and the image shift due to blank padding is $\rho_s = \rho \times \dfrac{\omega}{S_w}$.

On the other hand, when the angle of shearing is greater than the orthogonal angle $(\theta_s > \sigma)$, the amount of blank padding ρ can be derived from $\rho = L\left(\dfrac{\sin\theta_s}{\cos\theta_s}\right) - S_w$ and the image shift due to blank padding is $\rho_s = 0$.

5.2.2 Main-scan Shearing

Contrary to using raster correction to shear the image in the sub-scan direction, main-scan shearing uses swath correction method that changes the swath start positions for each swath. The data path in Spectrum uses the pulses from the quadrature encoder of main-scan actuation to generate an imaging clock that signals the laser head to put down pixels at the exact position on the media. The generation of the imaging clock is derived by dividing each period of the main-scan actuation signal into K pulses of equal intervals via a phase lock loop scheme. Thus, each period of the imaging clock is equivalent to $(\dfrac{r_m}{K})$ μm of main-scan distance where r_m is the resolution of the main-scan actuation. Spectrum has $K = 64$ and $r_m = 45\mu m$ thus each period of the imaging clock is

equivalent to 0.7μm of main-scan travel. The imaging start signal, which signals the start and the end of a swath, is derived from counting the number of imaging clock periods from the index pulse of the main-scan actuation. The relationships among the signals are illustrated in Figure 45.
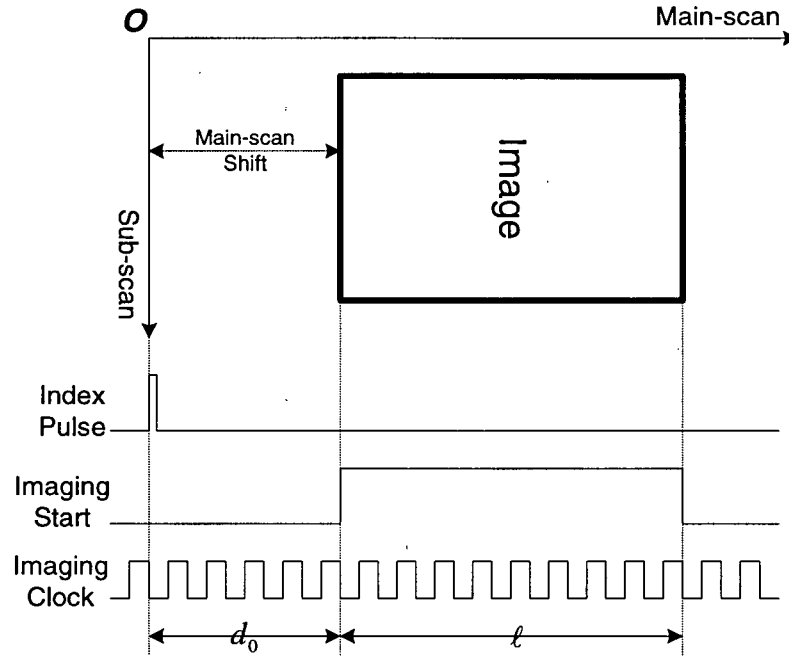
Figure 45 Imaging Signals

As shown in Figure 45, the main-scan shift image from the sub-scan axis is d_0 imaging clock periods and the imaging of a swath lasts ℓ periods.

To shear the image in the main-scan direction, the amount of shearing per swath in μm is:

$$\lambda = \omega \tan \theta_m = \omega \left(\frac{\sin \theta_m}{\cos \theta_m} \right) \qquad \text{Equation 32}$$

where ω is the width of a swath in µm. Equation 33 converts λ from µm into number of imaging clock periods

$$\varphi = \lambda \frac{K}{r_m} \qquad \text{Equation 33}$$

From above, the image clock periods from the index pulse to pulling the imaging start signal high for swath n is:

$$d_n = d_0 + (n-1)\varphi = d_0 + (n-1) \left(\omega \frac{\sin \theta_m}{\cos \theta_m} \right) \left(\frac{K}{r_m} \right) \qquad \text{Equation 34}$$

Using the orthogonal correction example shown in section 5.2.1 , the effect of main-scan shearing is shown in Figure 46 and Figure 47.
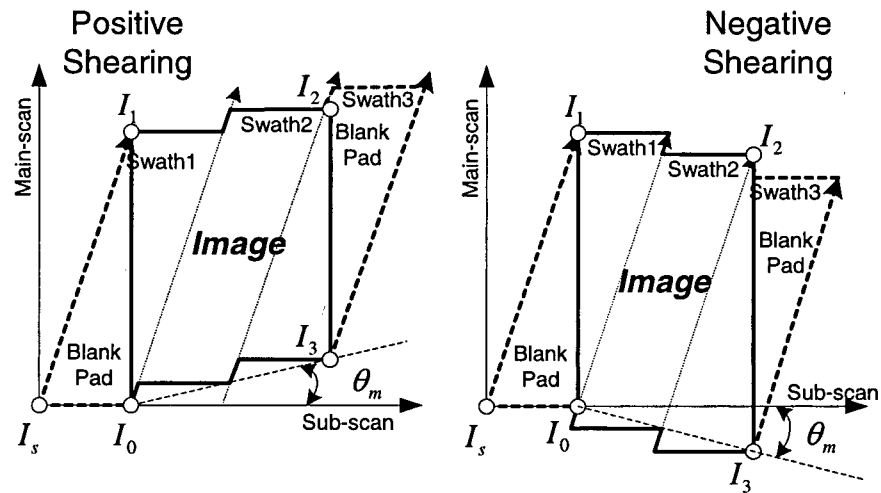
Figure 46 Positive and Negative Main-scan Shearing
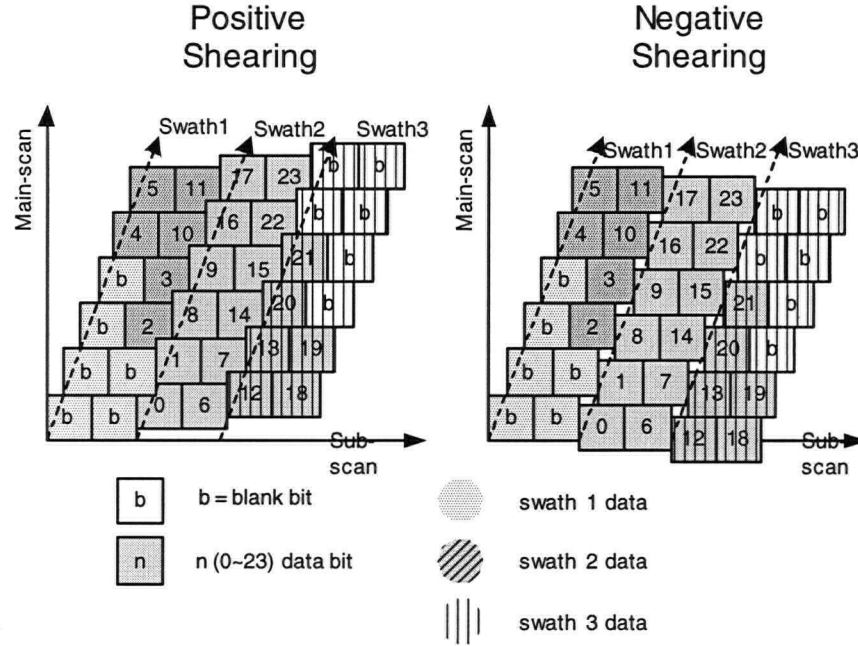
Figure 47 Expanded View of Main-scan shearing

To ensure the main-scan shifts from swath to swath do not produce observable artifacts, λ is limited to be less than the height of a single pixel. Since Spectrum produces pixels in the size of 10μm by 10μm, $|\lambda|$ must be less than 10μm. Using Equation 32, the maximum angle of main-scan shearing without observable artifacts on Spectrum is $|\theta_m| < 8325$μRad. Since $\theta_R = \theta_m$, the capability of the proposed rotation correction method is within ±8325μRad.

5.2.3   *Image Artifacts and Scaling Errors Due to Geometric Rotation*

Both the main-scan and sub-scan shearing algorithms have artifacts of less than one pixel in size, thus the image artifacts due to rotation correction are no more than 10μm. More specifically, artifacts due to sub-scan shearing are always 10μm

because it utilizes raster correction that manipulated the image data. Main-scan shearing artifacts, on the other hand, vary in sizes depending on the angle of shearing, but no larger than 10μm in any case. Because of the minute sizes of the artifacts, they cannot be observed by the naked eyes as demonstrated on the sample proof in Appendix A. To observe the image artifacts, several pictures are taken using 100X/200X/400X microscope as illustrated in Figure 48.
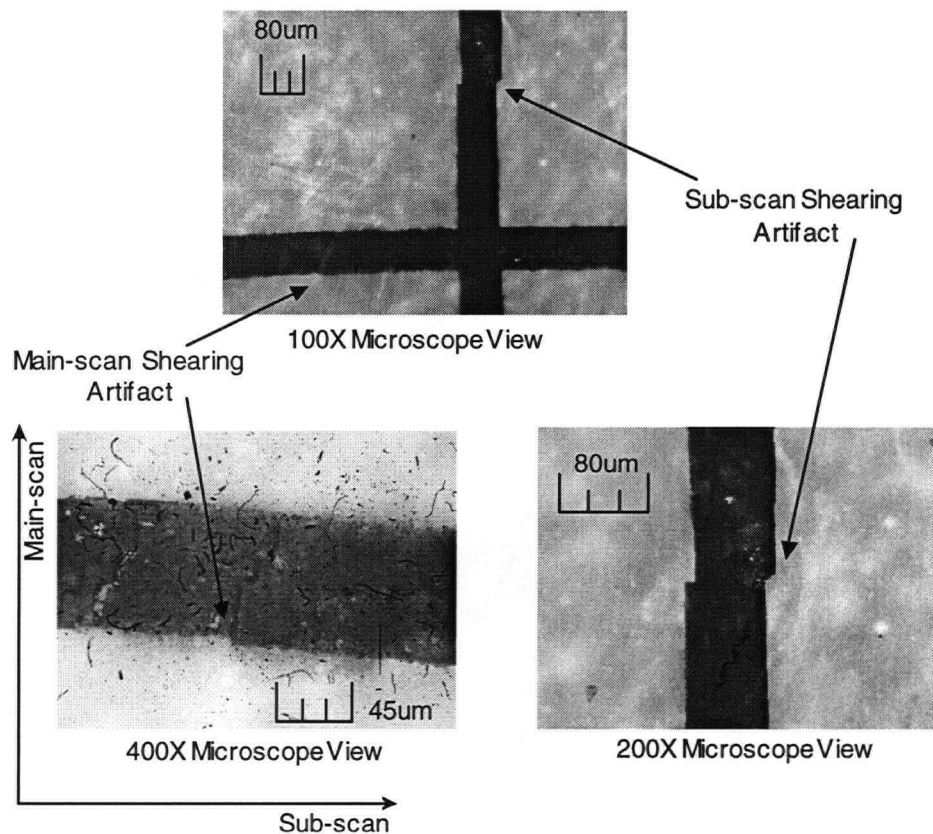
Figure 48 Microscopic Views of Image Rotation Artifacts

The sub-scan image artifact shown is 10μm (one pixel wide) in size and is visible under 100X microscope. On the other hand, the main-scan image artifact is approximately 2μm and is barely visible even under 400X microscope.

Another side effect of rotation correction is scaling error due to shearing operations that slightly expand the sheared edges of the image. The scaling error is illustrated in Figure 49.
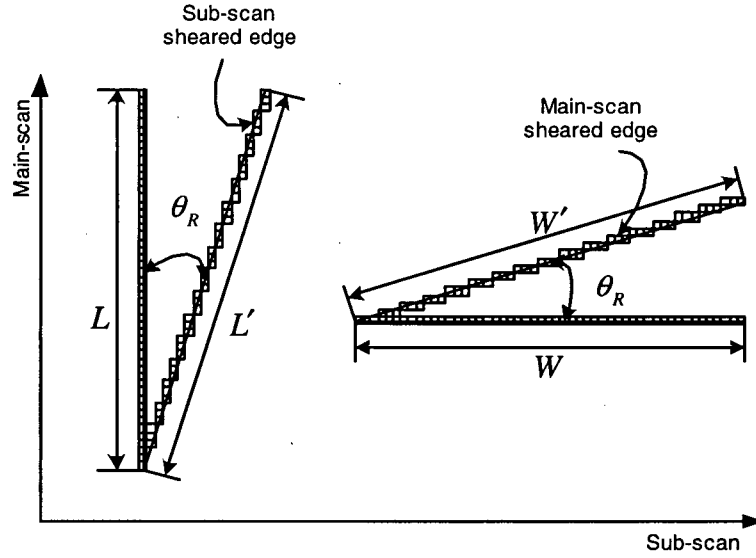
Figure 49 Illustration of Scaling Error

From Figure 49, the scaling of the image length is $L' = \dfrac{L}{\cos\theta_R}$ and the scaling of

the image width is $W' = \dfrac{W}{\cos\theta_R}$. The scaling factor Ω is defined as:

$$\Omega = \frac{1}{\cos\theta_R}$$

<div style="text-align:right">Equation 35</div>

In addition, the scaling error in the main-scan is defined as $L' - L = L(\Omega - 1)$ and the scaling error in the sub-scan is defined as $W' - W = W(\Omega - 1)$. When making a two-sided proof, the difference in the scaling errors from front to back affect

the accuracy of backup registration. Assuming the front image is rotated by θ and the back image is rotated by δ, the misalignments in backup registration due to scaling error are $L_1' - L_2' = L(\Omega_\theta - \Omega_\delta)$ in the main-scan and $W_1' - W_2' = W(\Omega_\theta - \Omega_\delta)$ in the sub-scan. The worst-case misalignment occurs when $|\Omega_\theta - \Omega_\delta|$ is maximized, or when $\||\theta| - |\delta|\|$ is maximized. Since $|\theta_R| < 8325\mu\text{Rad}$, the worst case occurs when one rotation angle is $8325\mu\text{Rad}$ while the other angle is 0. Therefore, the worst-case misalignments in backup registration due to scaling error in the main-scan is $26\mu\text{m}$ and the worst case scaling error in the sub-scan is $19\mu\text{m}$.

5.3   Raster Data Mirroring

To compensate for the flipping of the proof sheet, the back image must be plotted in a mirrored fashion. Since the proposed process flips the proof sheet with respect to sub-scan axis, the raster data of the back image must be mirrored accordingly. The proposed implementation of raster data mirroring on the Spectrum is by reversing the direction of raster data entering the data buffer. Figure 50 shows the normal and mirrored data buffering.
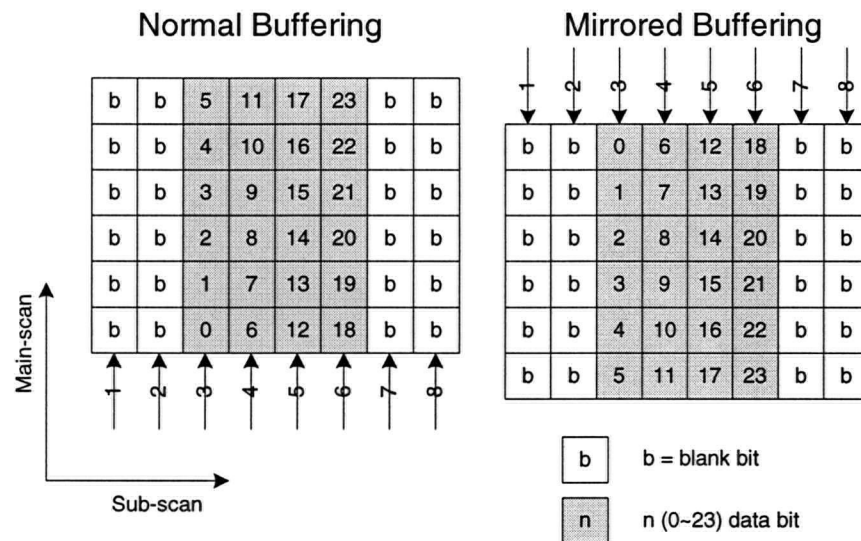
90

Figure 50 Normal and Mirrored Raster Data Buffering

By mirroring raster data in the buffer, the imaging schemes for the front and the back images are consistent thus simplify the proofing process.

Chapter 6

ANALYSIS OF RESULTS

In order to gauge the performance of the proposed automatic backup registration process in terms of registration accuracy, samples of two-sided proofs need to be produced and analyzed. Methods of measuring the amount of misalignment between the front and the back images need to be studied such that the misalignment can be quantified and analyzed. This chapter proposed three methods of measuring backup registration and compares the strengths and weaknesses in each method.

The population of sample proofs produced for this study is insufficient to establish an accurate limitation of the proposed backup registration process due to the high costs of digital thermal proofing media. Nevertheless, the registration at each corner of each image of each sample is examined to estimate the effectiveness of geometric correction. Finally, an estimation of the capability of the proposed backup registration process is presented.

6.1   Methods of Measuring Backup Registration

For the purpose of this study, 20 sample proofs, each with identical front and backside images, are produced. Portion of a sample proof is presented in Appendix A. To measure the misalignment between the front and backside images, three methods are tested.

1. By sight without optical aid. By placing the sample proof in front of a lamp, the image on the back of the proof sheet is revealed. To enhance

the backside image, two process colors with the most contrasts, namely magenta and black, are used for plotting the front and the back images respectively. Without magnification, one can gauge whether the images are with the specified 1mm backup registration tolerance because the sample proof contains a 1mm tick feature. However, since the misalignments are typically minute, some sorts of optical aid are needed to quantify the amount of misregistration.

2. By transparent window. By gluing a transparent film such as a receiver to a frame of paper, the composite proof sheet can be imaged on both sides. Because of the edges of the composite are made of paper, the geometric detection functions as if the composite were a sheet of paper. After imaging, the transparent portion of the composite is placed under a microscope and backup registration can be measured. Figure 51 shows the microscopic view of a sample composite proof.
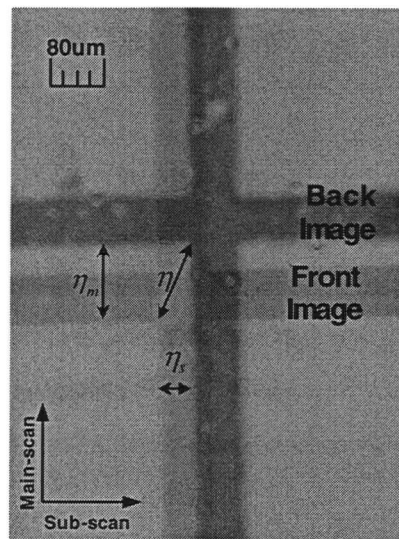

Figure 51 Measuring Backup Registrations with Microscope

As shown, the main-scan misregistration η_m is about 115μm while the sub-scan misregistration η_s is about 50μm. The total misregistration η can be derived from:

$$\eta = \sqrt{\eta_m^2 + \eta_s^2}$$ <div align="right">Equation 36</div>

Thus, in this example, η is about 125μm.

By using a microscope, the misalignments of front and backside images can be precisely measured. However, images done on the composite are different from images done on paper in terms of backup registration because of the surface of the composite during imaging does not lay flat on the carrier as paper does. This causes points on the composite to exhibit different misregistration compares to paper. Nevertheless, the result measured can be used to check how close the backup registration meets the specification.

3. By scanner. The images on both sides of the sample proof are scanned as digital images by using commonly available desktop scanner. In addition, two registration holes near the corner of the sample are punched. Using digital imaging tools such as Adobe Photoshop, the scanned images can be super-imposed on top of each other as shown in Figure 52.
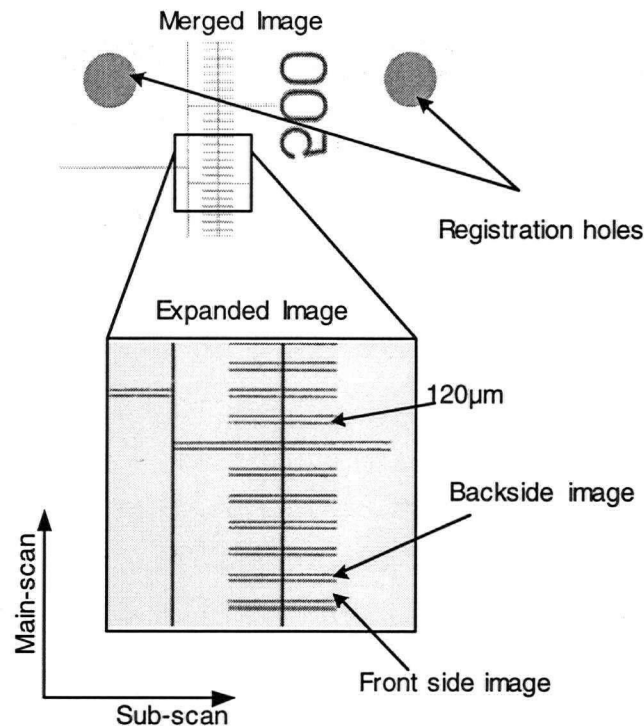
Figure 52 Measuring Backup Registration using Scanned Images

From the resulting image, any misalignment can be measured as precisely as the scanning resolution. In the example shown, a 600dpi scanner is used thus the precision is about 40μm. Therefore, in this example, η_m is three pixels or 120μm. The sub-scan misregistration is not visible because it is less the 1 pixel or 40μm. Although not as precise as using the microscope, the results measured via this method are sufficient for checking backup registration.

The results presented in the following section are obtained by the scanner methods.

6.2 Backup Registration Analysis

To quantify the misregistration, two points I_0 and I_2 at the corners of the image on each sample proofs are measured. Being the image origin, the misregistration at I_0 is likely to be caused by error due to geometric detection, specifically sub-scan edge detection. Figure 53 illustrates the distribution of misregistration at I_0 from the population of 20 samples.
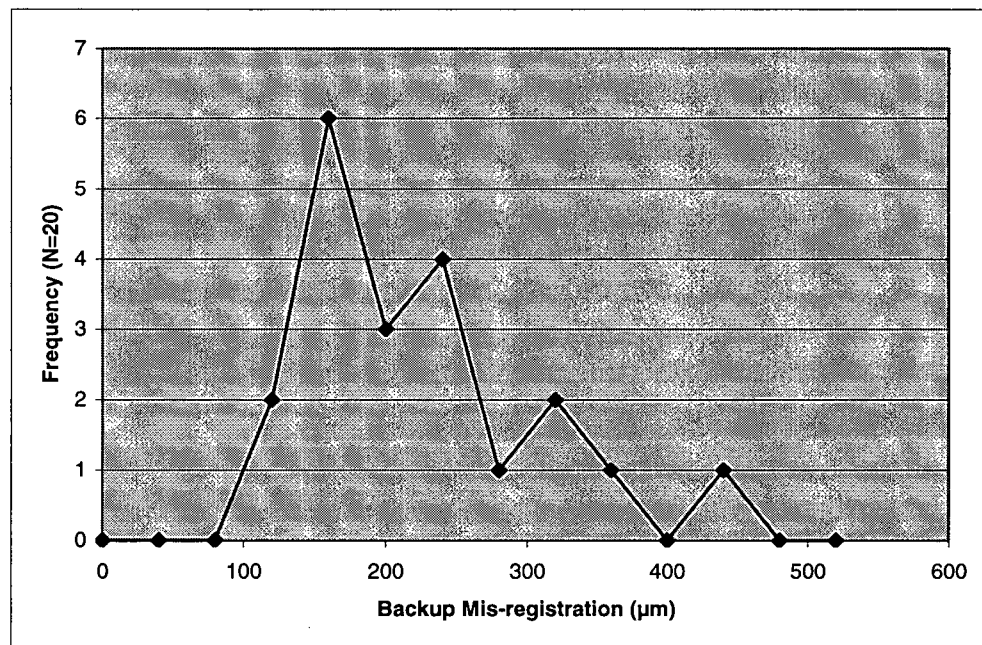

Figure 53 Distribution of Misregistration at I_0

The misalignments at I_0 are mainly in the main-scan direction, while the sub-scan errors are unobservable. This is as expected since the sub-scan shifts are significantly more accurate than the main-scan shift when measured by the geometric detection process. All sample proofs are registered within 500μm with the average of 294μm.

96

At the far side corner I_2, the cumulative errors due to rotation correction contribute to the total misregistration. In Figure 54, the distribution of misregistration at I_2 from the population of 20 samples is shown.
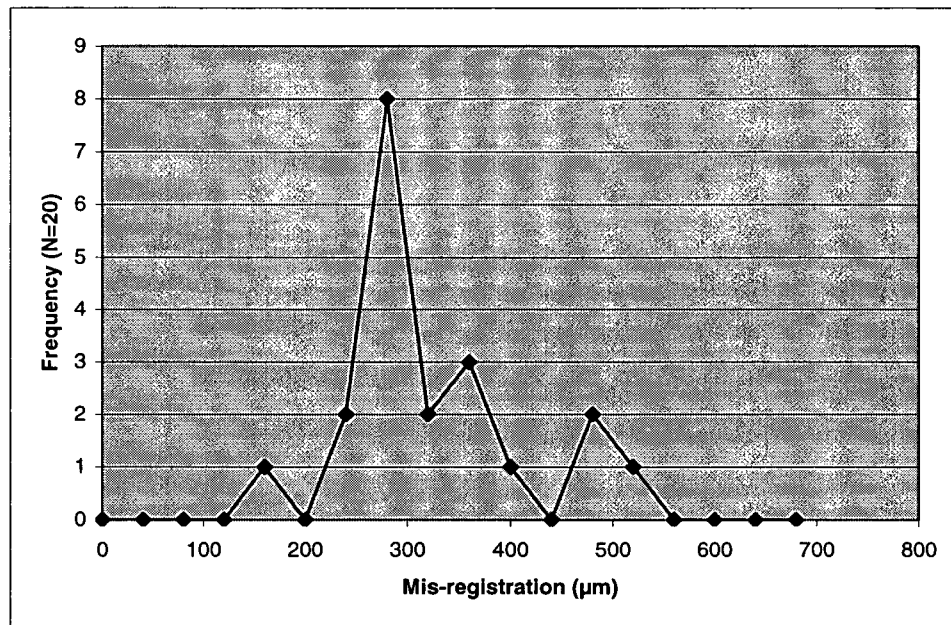
Figure 54 Distribution of Misregistration at I_2

The misalignments at I_2 are larger compares to I_0 with both main and sub-scan errors. Even though main-scan errors are still the main contributors to the misalignments, sub-scan errors are observable but less than 160μm. The average of the total misalignments is 350μm and all samples are registered within 550μm.

To measure the effectiveness of the rotation correction, the differences between the front and the back image rotation angles (angular offsets) are plotted against the misregistrations at I_2, and is shown in Figure 55.
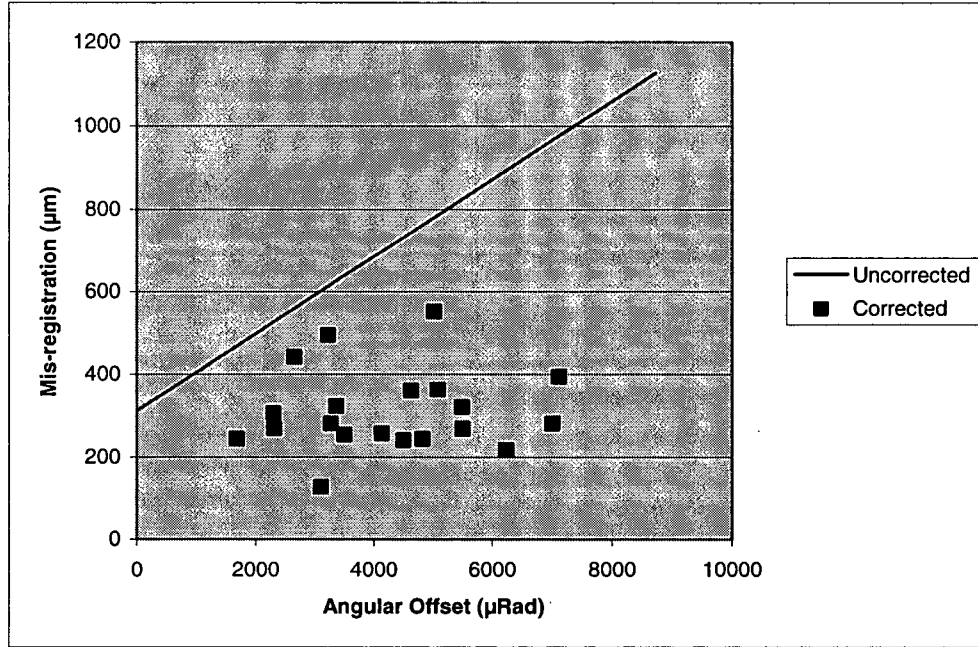
Figure 55 Angular Offsets vs. Misregistrations at I_2

The angular offset α is defined as

$$\alpha = \left\| |\theta| - |\delta| \right\|.$$

The uncorrected line in Figure 55 represents the theoretical misregistration E_t assuming no rotation correction. The misregistration is calculated from

$$E_t = \overline{E} + \alpha\sqrt{L^2 + W^2}$$

where $\overline{E}$ is the average misregistration at I_2 and $\sqrt{L^2 + W^2}$ is the offset from I_0 to I_2. The corrected series in Figure 55 are the measured misregistrations at I_2 with rotation correction and they do not follow the linear growth of E_t.

Therefore, the misregistration caused by angular offset is effectively minimized by rotation correction.

All the 20 sample proofs have backup registration within 550μm and are within the 1mm as required.

Chapter 7

CONCLUSIONS

A novel method of automatic backup registration has been proposed for digital thermal halftone proofing. The proposed method manipulates the front and back images of a two-sided proof to compensate for the variations in the handling of proof sheets. Unlike mechanical registration, the proposed method does not require precise mechanical hardware for paper handling, thus, can be implemented on existing proofing devices such as the Spectrum proofer. The proposed method consists of two processes: geometric detection and geometric correction. These two processes are studied by implementation on the Spectrum proofer and the results are summarized in the section 7.1 and 7.2. The overall accuracy of the backup registration achieved by the two processes, including methods used to quantify the results, are summarized in section 7.3. Finally, some suggestions for future work to improve the proposed method are offered in section 7.4.

7.1   Geometric Detection

The geometric detection process detects shifts and rotations of the proof sheet when it is loaded in the device. The process is implemented on the Spectrum by using the focus laser system to detect the edge positions of the proof sheet. For the process to detect the required parameters, it must be able to distinguish between the proof sheet and the carrier reliably. Since the carrier has similar surface reflectivity as the proof sheet, methods of modifying the carrier surface to either diffuse or absorb the reflected light are investigated. Among the four methods studied, spraying the carrier with flat black paint to create a smooth

non-reflective surface is the most effective one. With the modification, a threshold can be chosen for the algorithm to distinguish between the carrier and the proofing sheet with 99.5% of success rate. To simulate the performance of the modified carrier under non-ideal sensing conditions, the power of the incident laser beam is reduced to conduct the tests. The test results are comparable with those under optimal sensing conditions. Studying signal profiles near the edges of the proof sheet reveals the difference in the main and sub-scan edge characteristics due to paper curls near the sub-scan edges. The edge curls affect the accuracy of the sub-scan edge detection by 95μm and must be accounted for in geometric correction.

The algorithm for geometric detection is implemented as embedded software routines on two micro controllers. Due to the lack of computing resources, the algorithms are designed to be efficient by simplification.

The results from repetitive tests of geometric detection show that the process can detect the main-scan edge positions with variation of less than 5μm and the sub-scan edge positions with accuracy of 300μm. Since the results are well within the required 1mm backup registration accuracy, the geometric detection process is capable of providing the parameters needed for the geometric correction process reliably.

7.2   Geometric Correction

The geometric correction process shifts and rotates the images to align them from the front side to the backside of the paper. To properly shift the images, the following factors must be considered:

- The main-scan shift consists of curl effect, image margin height, and the main-scan distance between the write laser and the focus laser.

101

- The sub-scan shift consists of image margin width, the blank padding shift, and the sub-scan distance between the write laser and the focus laser.

The rotation of the image is done by two operations: main-scan shearing and sub-scan shearing. The implementation for main-scan shearing on Spectrum uses the existing orthogonal correction algorithm that manipulates the raster data buffered prior to imaging. The ability to support the various shearing angle in the orthogonal correction algorithm is added so the image can be rotated by any amount.

Unlike main-scan shearing, the proposed sub-scan shearing algorithm controls the timing of imaging start for each swath instead of manipulating the raster data. Thus, the integrity of the raster data is maintained and the image artifacts caused by rotation are minimized. On the other hand, the total amount of shearing must be distributed evenly between swaths, so it is impossible to do significant sub-scan shearing while keeping the imaging artifacts to a minimal. Therefore, the maximum angle of image rotation is limited at $\pm8325\mu$Rad for Spectrum. The artifacts caused by image rotation are negligible and unobservable.

For imaging the data in a mirrored fashion with respect to the sub-scan axis, the proposed method reflects the image by reversing the direction of the raster data entering the swath buffer.

7.3 Accuracy of Backup Registration

To quantify the accuracy of the proposed method, three different ways of measuring backup registration are tested:

1. By sight without optical aid. Placing a two-sided proof in front of a light source reveals the image on its back. This method can gauge whether the

images meet the specified 1mm backup registration but cannot quantify the amount of misregistration.

2. By transparent window. This method plots images on both sides of a composite proof sheet with a transparent film glued to a paper frame. This method allows backup registration to be measured using microscope but the results are inconsistent comparing to images done on paper because of the uneven surface of the composite during imaging. Nevertheless, the results measured can be used for checking whether the backup registration requirement is met.

3. By scanner. By punching two registration holes near the corner of the proof, scanning the corner, then digitally merging the scanned images, the accuracy of backup registration can be measured precisely depending on the scanning resolution. The disadvantage of this method is the amount of time and labor required for processing the scanned images.

Out of the twenty proofs produced, the overall backup registration is within $550\mu m$. Since the result is better than the requirement by approximately 45%, the proposed method has the potential for commercial applications.

7.4 Recommendation for Future Work

The following issues may be addressed by future research:

- The population of proofing samples examined for this research is limited due to the difficulty of obtaining proofing media. To better understand the reliability of the proposed process, a large quantity of proofs needs to be produced and examined, preferably in a production environment.

- For platform lacking the necessary detection mechanism, a low cost digital camera may be used in place of the focus laser system. By processing the captured images of the corners of the proof sheet, it may be possible to achieve better accuracy while reducing the amount of time needed for geometric detection.

- Modification of the mechanical system may be able to reduce or eliminate the edge curl effect for better backup registration accuracy.

- The process of using scanners to measure the backup registration may be automated in future research to reduce the processing time and the labor required.

Bibliography

[1] M. H. Bruno, *Pocket Pal: A Handbook for Graphic Art Production*, 17th Edition, International Paper, Memphis, T.N. (1997).

[2] W. L. DeMarco, The Value of Digital Halftone Proofing. *PIRA Proofing Confrence*, 52-78 (1999).

[3] L. Cottrell, *Print Publishing Guide*, Adobe Press, San Jose C.A. (1998).

[4] L. Leland, Converting the Masses. *Graphic Arts Monthly*, 44-50 (February 2001).

[5] F. J. Romano, *Guide to Digital Prepress*, Delmar, Albany N.Y. (1996).

[6] S. Hoover, Closing the Color-Control Loop. *Journal of American Printers*, **4**, 34-38 (2001).

[7] R.F.V. Anderson, *Introduction to Linear Algebra*, Holt, Rinehart and Winston, Canada (1986).

[8] R.E.Walpole and R.H. Myers, *Probability and Statistics for Engineers and Scientists*, 4th Edition, Macmillan, New York, N.Y. (1989).

Appendix A. Sample of Two-Sided Digital Thermal Proof

The next page is a portion of 22 by 30 inch, two-sided digital thermal proof. The long side is the main-scan direction while the short side is the sub-scan direction. The magenta is used for the front side image while the black is used on for the backside image. The rotation correction angle for the front side image is $1353\mu Rad$ and $-3474\mu Rad$ for the backside. The backup registration is within $280\mu m$.

Appendix B. Algorithm Design Specifications for Geometric Detection

The following functions are implemented in the head controller.

HC_EdgeDetectionControl()

Purpose	Control the edge detection sequences in the head controller
Interrupts	Enable
Prototype	int HC_EdgeDetectionControl(uint TimeoutInMs)
Description	Once called, turn on the focus laser generator, enable the A/D converter sampling, pull down the threshold crossing line , and enable the threshold comparison interrupt. Loop until the threshold-crossing event occurs or until timeout. Disable the A/D converter, turn off the focus laser generator, and pull down the threshold crossing line before exit. If timeout has occurred, disable the threshold comparison interrupt as well.

Arguments	Meaning
TimeoutInMs	The maximum duration in millisecond for the threshold crossing to occur after enabling the threshold comparison interrupt.

Return Values	Meaning
SUCCESS	A threshold-crossing event has occurred within the specified timeout.
TIMEOUT	No threshold-crossing event occurred within the specified timeout.
FAILURE	Fail to enable/disable A.D converter, fail to enable of Threshold Comparison ISR, or fail to turn on/off the focus laser generator.

_ISR_HC_ThresholdCompare()

Purpose	Interrupt service routine to compare the current sampled value with the threshold.
Invoked By	Raising edge of AD_Ready
Interrupts	Disable
Prototype	void _ISR_HC_ThresholdCompare(void)
Description	Upon entry, compare the AD_Sample with the threshold. If AD_Sample is less than the threshold, do nothing and exit. Otherwise, pull up the threshold crossing line and disable threshold compare interrupt.

The following functions are implemented in the main controller.

MC_GeometricDetection()

Purpose	Control the sequence of geometric detection
Interrupts	N/A
Prototype	int MC_GeometricDetection(boolean FrontSide, GC_PARAM * Param)
Description	Depending on FrontSide, move the focus laser to the start positions for edge detection, then call MC_MainScanEdgeDetect() and MC_SubScanEdgeDetect() to obtain the edge positions. If the edge detections are successful, then calculate the results and write to Param.

Arguments	Meaning
Side	The side of the proof sheet loaded. FrontSide =TRUE indicates the front side of the proof sheet is to loaded. Any other value indicates the backside of the proof sheet is loaded.
*Param	Pointer to a GC_PARAM structure that the results of the geometric detection are to write to. The results include main-scan offset in μm, sub-scan offset in μm, and rotation in μRad.

Return Values	Meaning
SUCCESS	Geometric detection is done successfully.
INVALID_RESULT	Indicate the calculated shifts or rotation is outside the boundary.
FAILURE	Error occurs while performing edge detections.

MC_MainScanEdgeDetect()

Purpose	Detect the main-scan edge position.
Called By	MC_GeometricDetection()
Interrupts	Enable/Disable
Prototype	int MC_MainScanEdgeDetect(POSITION *Edge)
Description	Upon entry, enable the threshold crossing interrupt and invoke HC_EdgeDetectionControl(). Send move command to the sub-scan actuation for a pre-determined distance. Loop while polling the threshold-crossing event until the event occurs or until the sub-scan actuation finished moving. If the threshold-crossing event has occurred, query the latched edge position, write to *Edge, then return SUCCESS. Otherwise, disable the threshold crossing interrupt and return FAILURE.

Arguments	Meaning
*Edge	The coordinate of the detected edge position in μm.

Return Values	Meaning
SUCCESS	Edge position detected successfully.
FAILURE	Edge position not detected.

MC_SubScanEdgeDetection()

Purpose	Detect the sub-scan edge position.
Called By	MC_GeometricDetection()
Interrupts	Enable/Disable
Prototype	int MC_SubScanEdgeDetect(boolean Direction, POSITION *Edge)
Description	Upon entry, enable the threshold crossing interrupt and invoke HC_EdgeDetectionControl(). Depending on Direction, send positive or negative move command to the main-scan actuation for a pre-determined distance. Loop while polling the threshold-crossing event until the event occurs or until the main-scan actuation finished moving. If the threshold-crossing event has occurred, query the latched edge position, write to *Edge, then return SUCCESS. Otherwise, disable the threshold crossing interrupt and return FAILURE.

Arguments	Meaning
Direction	Direction=TRUE indicates the sub-scan edge is above the starting position and shall search the edge in the positive main-scan direction. Otherwise, the sub-scan edge is below the starting position and shall search the edge in the negative main-scan direction
*Edge	The coordinate of the detected edge position in μm.

Return Values	Meaning
SUCCESS	Edge position detected successfully.
FAILURE	Edge position not detected.

_ISR_MC_ThersholdCrossing()

Purpose	Interrupt service routine to monitor the threshold crossing line.
Invoked By	Raising edge of threshold crossing line.

Interrupts	Disable
Prototype	void _ISR_MC_ThresholdCrossing(void)
Description	When invoked, latch the current position of the main and sub-scan actuation, disable the threshold crossing interrupt, and set the threshold-crossing event bit.